PERGAMON

Journal of Structural Geology 23 (2001) 355–378

JOURNAL OF STRUCTURAL GEOLOGY

www.elsevier.nl/locate/jstrugeo

Folding by cataclastic flow at shallow crustal levels in the Canyon Range, Sevier orogenic belt, west-central Utah

Zeshan Ismat*, Gautam Mitra

Department of Earth and Environmental Sciences, University of Rochester, Rochester, NY 14627, USA

Received 18 January 2000; accepted 30 June 2000

Abstract

Folds form by ductile deformation typically involving continuous flow. In the elastico-frictional regime, such deformation may be accomplished by cataclastic flow involving collective movement on a population of fractures and zones. The Canyon Range (CR) syncline, part of the CR thrust sheet in west-central Utah, developed in this regime. The CR syncline is composed of thick-bedded quartzite units with a small material contrast between layers, limiting limb rotation by flexural slip alone. Thus, fracture populations developed to accommodate fold tightening by limb rotation and thinning, and the formation of transverse zones across the fold. Several generations of fracture and deformation zone (DZ) networks are recognized from mesoscopic and microscopic evidence, and can be related to stages of folding. The net result of the large number of distributed fractures and deformation zones is a continuous deformation that is homogeneous at the scale of the outcrop. All these lines of evidence suggest that large-scale cataclastic flow accommodated folding by allowing rigid mesoscopic blocks to slide along bounding DZs.

Along its length, the CR syncline consists of several segments bounded by transverse zones with different mechanisms accommodating fold tightening in adjacent segments. In one segment, fold tightening progressed by limb rotation, and then out-of-the-core thrusting. In contrast, fold tightening in the adjoining segments occurred by rotation and thinning of one limb and possible hinge migration, with the steeply dipping to overturned limb showing progressive thinning of units on a megascopic scale and progressive increase in the thickness and density of deformation zones at all scales.

1. Introduction

Fold tightening occurs by ductile deformation typically involving continuous flow. Such deformation is common at deep crustal levels where high temperatures allow plastic deformation mechanisms to dominate. However, ductile deformation may also occur at shallow crustal levels under elastico-frictional conditions by cataclastic flow, a process that involves blocks of various sizes sliding past each other along a stable network of fractures and deformation zones (DZs). Although individual fractures and DZs are discrete and zonal discontinuities, the collective character of a fracture network allows an overall ductile deformation at the largest scale (Twiss and Unruh, 1998). Analogy to the deformation of a bean-bag is apt, with the external shape changes of the bean-bag being accommodated by beans frictionally sliding past each other within the bean-bag. Thus, at shallow crustal depths, large-scale fold tightening may be accomplished by collective movement on a population of fractures and deformation zones, at all scales, allowing blocks to slide past one another for a continuous deformation at the largest scale. The terminology to describe such deformation can be confusing, so we summarize the principal terms below.

We use terminology developed over the last 25 years (Sibson, 1977; Mitra, 1978, 1984, 1992; Paterson, 1978; Ashby et al., 1979; Schmid, 1982; Tullis et al., 1982; Hadizadeh and Rutter, 1983; Rutter, 1986; Schmid and Handy, 1991; Twiss and Moores, 1992). The terms "brittle" and "ductile" are phenomenological terms that are a function of the scale of observation. The classical definition of "brittle fracture" refers to failure of rock at a certain stress. In experimental deformation, a significant stress drop occurs as cohesion is lost during fracturing (Paterson, 1978; Twiss and Moores, 1992); no deformation mechanisms are specified. While fracture at the grain scale may be preceded by elastic deformation alone (Griffith, 1920), it may also be a result of significant amounts of plastic deformation (Mitra, 1978; Ashby et al., 1979). Throughgoing fractures form by coalescence of grain-scale cracks, thus requiring additional deformation beyond initial cracking, which may also involve significant amounts of plastic deformation (Ashby et al., 1979). Thus, "brittle fracture" can imply different

* Corresponding author.
E-mail address: zlsm@mail.rochester.edu (Z. Ismat).

0191-8141/01/$ - see front matter
PII: S0191-8141(00)00101-2

mechanisms at different scales. In naturally deformed rocks, the presence of cracks at the grain scale does not necessarily imply that a throughgoing fracture developed (Mitra, 1992), and may imply "brittle" or "ductile" deformation.

"Ductility" refers to a material's ability to flow uniformly and its capacity for substantial, non-localized strain, but it does not specify mechanisms for deformation (Schmid, 1982; Rutter, 1986). A material can deform in a ductile manner through three classes of mechanisms: (1) intracrystalline plasticity, (2) diffusive mass transfer, and (3) cataclastic flow, or by various combinations of all three (Hadizadeh and Rutter, 1983; Schmid and Handy, 1991). Cataclastic flow refers to the pervasive fragmentation of a material, fragment rotation, frictional sliding and dilatancy (Sibson, 1977; Paterson, 1978). So, a material can lose cohesion (i.e. behave in a "brittle" manner) and still flow continuously (behave in a "ductile" manner). Fundamental to cataclastic flow are stabilizing factors (e.g. mechanically and physically hardened zones) to allow selective use and development of a stable penetrative network of fractures and deformation zones (Hadizadeh and Rutter, 1983). Although, cataclasis and cataclastic flow were originally defined at the grain scale, the same elastico-frictional mechanisms may operate at all scales (Sibson, 1977).

It is better to discuss the origin of different structures with reference to deformation mechanisms (Rutter, 1986; Schmid, 1982; Schmid and Handy, 1991; Twiss and Moores, 1992). Cataclasis includes fracturing after elastic deformation and frictional sliding on fractures. It can lead to brittle failure (throughgoing fracture or fault) or ductile deformation (cataclastic flow). The mechanism is pressure dependent and dominant at shallow crustal levels; following Sibson (1977) we refer to this behavior as occurring in the Elastico-Frictional (EF) regime. At deeper crustal levels, thermally activated mechanisms (intracrystalline plasticity and diffusive mass transfer) dominate in the Quasi-Plastic (QP) regime (Sibson, 1977). Based on laboratory experiments, the boundary between the EF and QP regime for quartz-rich rocks is ~250–300°C (Sibson 1977), which is equivalent to ~10–15 km depth for a normal geothermal gradient of ~25°C/km. The EF/QP transition is a physical boundary, unlike a "brittle–ductile" boundary, and its position is a function of temperature, pressure, grain size, mineralogy, water content, etc. (Sibson, 1977), and may change during progressive deformation.

A transition from dominantly plastic deformation processes to elastico-frictional processes might be expected in any setting where rocks are progressively brought to the surface during continuing deformation. The internal portions of any fold and thrust belt (FTB) must be continuously reactivated and progressively brought to the surface by uplift and erosion to maintain critical taper in an evolving wedge (DeCelles and Mitra, 1995). In addition to out-of-sequence imbrication, fault reactivation and duplex growth (e.g. Boyer, 1992; DeCelles, 1994; Boyer and Elliott, 1982; Schonborn, 1992), fold tightening (Mitra and Sussman, 1997) helps to achieve the required wedge thickening. As rocks are brought closer to the surface into the elastico-frictional regime by progressive uplift and erosion, faulting and fold tightening are accommodated by cataclastic flow. While the importance of cataclastic flow in the evolution of fault zones and thrust sheets is well documented (e.g. Wojtal, 1989; Wojtal and Mitra, 1986, 1988; Mitra, 1984, 1992; Yonkee and Mitra, 1993; Evans 1993), very little work exists on its role in fold tightening at shallow crustal levels (e.g. Wise, 1964; Prucha et al., 1965; Stearns, 1975, 1978).

Some previous work has been done on the geometric and dynamic relationship between folding and fracturing. Instantaneous fracturing at some stage during plane strain folding with the fractures forming under the same stress system that gave rise to the fold was typically assumed (Price, 1966 Price 1967; Hancock 1985). Also, simple direct correlations are made between laboratory-based deformation experiments on isotropic material and field observations (Etchecopar et al., 1981; Hadizadeh and Rutter, 1983) without accounting for material heterogeneities and scale incompatibilities. Such analysis is inadequate for explaining complex fracture networks associated with tight folds, where many superposed increments of fracturing develop during fold growth in a three-dimensional strain field, not just at one instant during folding.

Little detailed work has been done on the kinematics of natural folding with cataclastic flow and distributed fracture networks within the elastico-frictional regime. Some studies identified fractures and faults formed during successive phases of fold tightening on the basis of fracture characteristics and cross-cutting relationships (e.g. Price, 1967; Jamison and Stearns, 1982). However, these studies emphasized the collective character of the entire fault population in relation to folding and did not address the implications of the temporal evolution of the fault populations for the kinematics of folding. Other attempts at separating deformation phases were based on fracture and slip orientations produced in the laboratory (e.g. Etchecopar et al., 1981) which do not adequately explain the complexities of natural systems (Bott, 1959; Etchecopar et al., 1981). Early work studying the role of cataclastic flow as a mechanism for producing folds (Stearns, 1978; Hadizadeh and Rutter 1983; Rutter 1986) showed that small, homogeneously distributed movements on a population of bounding fractures and deformation zones, accommodate strains. However, these studies dealt with large wavelength, open folds.

We attempt to define more precisely the structural association between the evolution of fracture networks and large-scale progressive fold tightening by addressing three questions:

1. How does the fracture-network pattern vary relative to position on the fold and what does this variation tell us about changes in the deformation field across the fold?

2. Do the fracture networks change as the fold progressively tightens?
3. What do the variations in large-scale brittle strains tell us about the bulk mechanical behavior during folding by cataclastic flow?

We use the answers to infer the bulk mechanical behavior of large folds during progressive tightening by pervasive brittle fracturing.

We have studied the relationship between folding and fracturing in the Canyon Range, west-central Utah. In this area, uniform lithologic composition of beds involved in folding, variation of fold geometry along strike, well constrained timing relationships of progressive fold growth, and superbly exposed fracture networks, provide an ideal setting for analyzing the relationship between fracturing and folding in the internal portion of a FTB and its role in maintaining critical taper. The results have larger implications for evaluating the role of fracture networks in folding and fold tightening in other structural settings.

2. Geologic background

2.1. Regional geology and evolution of the Canyon Range

The Sevier fold-and-thrust belt (FTB) defines the eastern margin of thin-skinned deformation in the Cordilleran orogen of western North America (Fig. 1) (Armstrong, 1968; Burchfiel and Davis, 1975; Miller et al., 1992; Allmendinger, 1992). In this belt, Proterozoic, Paleozoic and Mesozoic miogeoclinal rocks were transported eastward during the late Cretaceous (55–140 Ma) Sevier orogeny (Armstrong, 1968; Burchfiel and Davis, 1975; Schwartz and DeCelles, 1988). The Sevier FTB is composed of a series of segments, or salients, bounded by transverse zones that strike at high angles to the trend of the belt. The Central Utah segment (Fig. 1) has four major thrusts: (from west to east) Canyon Range, Pavant, Paxton and Gunnison (Christiansen, 1952; Armstrong, 1968; Burchfiel and Hickcox, 1972; Higgins, 1982; Lawton, 1982, 1985; Standlee, 1982; Allmendinger et al., 1983; Holladay, 1983; Millard, 1983; Villien and Kligfield, 1986; Pequera, 1991; Royse, 1993; Pequera et al., 1994; Mitra et al., 1994, 1995; Coogan et al., 1995; DeCelles et al., 1995; Sussman, 1995; Sussman and Mitra, 1995a,b; Lawton et al., 1997). The thrust sheets are fragmented by Tertiary Basin-and-Range normal faulting (Fig. 1).

The Canyon Range in west-central Utah exposes mainly Proterozoic quartzites of the Canyon Range (CR) thrust sheet (Fig. 2). The sheet is folded into a large-scale anticline–syncline pair. Tightly folded Cretaceous synorogenic Canyon Range conglomerates are preserved in the core of the Canyon Range syncline, and overlie Cambrian quartzites and carbonates along a folded erosion surface. CR footwall rocks of the underlying Pavant sheet are exposed both along the CR thrust trace on the eastern flank of the range and in an erosional window through the anticline on the western flank of the range (Fig. 2). The CR thrust also overrides its own synorogenic conglomerates along portions of its trace on the eastern flank of the range (Fig. 2).

The evolution of deformation conditions in the CR through time is well constrained on the basis of a balanced regional cross section (Coogan et al., 1995; Mitra, 1997) and a well defined erosion and deformation history obtained from provenance information on Cretaceous synorogenic sedimentary rocks (DeCelles et al., 1995; Mitra, 1997; Lawton et al., 1997). Initial deformation of the Proterozoic quartzites of the CR thrust sheet occurred under deep ($>$15 km) conditions at the time of its initial emplacement (Fig. 3). The sheet was folded as it moved over a ramp in the Pavant thrust (PVT), and continued to be eroded down to the level of the Proterozoic–Cambrian quartzites before some conglomerates were preserved in the core of the broad syncline. Since these conglomerates ($<$2 km thick) were folded during subsequent stages of tightening of the syncline, the deformation of the underlying quartzites must have occurred under a shallow overburden ($<$5 km), well within the elastico-frictional regime for quartzites (Sibson, 1977; Smith and Bruhn, 1984; Mitra, 1997).

Fold tightening occurred while the CR thrust sheet was being deformed by motion on younger thrusts below and in front of the Canyon Range thrust (CRT). The CRT was continually reactivated as slip was transferred to the CRT by means of a connecting splay duplex (Mitra and Sussman, 1997) between the lower Pavant thrust (PVT) and the upper CRT (Fig. 2). The duplex forms the core of the CR anticline and duplex growth was directly responsible for amplification of the anticline and tightening of the adjoining syncline from an open fold to a tight, overturned fold.

In summary, much of the fold tightening in the CR thrust sheet occurred during the later part of the Sevier orogeny under shallow overburden, within the elastico-frictional regime. The rocks developed "fracture networks" which include both extensional and shear fractures and deformation zones (DZs) with a significant component of shearing displacement. These Sevier-age deformation features are used to determine the kinematic history of CR folding. They can be easily distinguished from open fractures associated with Tertiary normal faults.

2.2. The Canyon Range syncline

The CR syncline trends approximately N–S and its geometry changes along strike, from an open fold with no plunge at its southern end to a tight and then overturned fold with a $>45°$ plunge toward the NNW at its northern end (Figs. 2 and 4). The CR thrust in the west limb steepens northward and is likewise overturned at the northern end of the range.

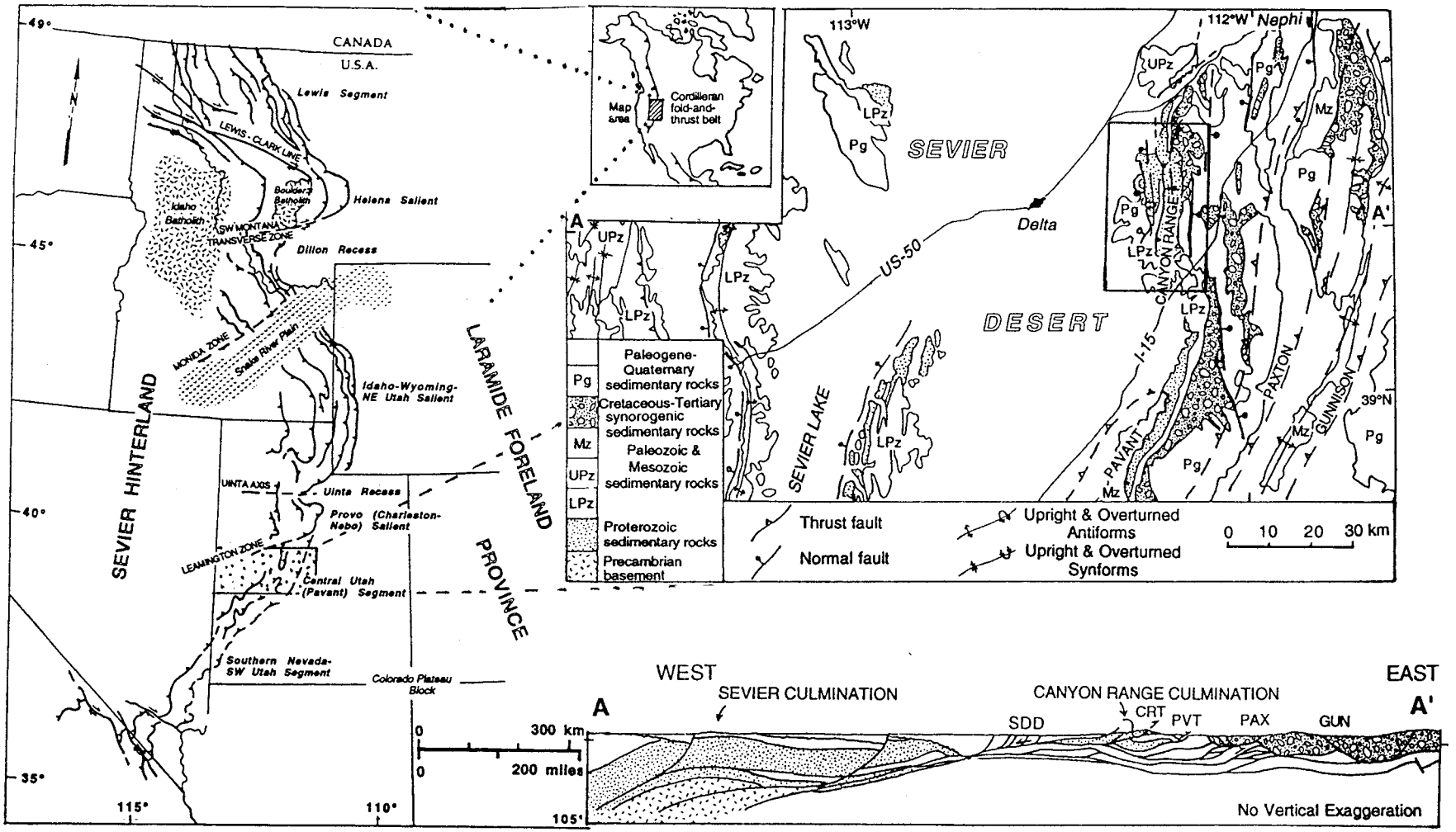

Fig. 1. The Sevier fold and thrust belt of the western USA with principal salients and recesses, and the transverse zones bounding them. Detailed map shows generalized geology of central Utah with the major Sevier-age structures exposed in the ranges of the Basin-and-Range province (after Hintze, 1988). Location of Fig. 2 and line of regional cross-section (A–A′) are shown. The cross-section along A–A′ (after Coogan et al., 1995) shows the major structures: Sevier culmination, Canyon Range culmination, CRT (Canyon Range thrust), PVT (Pavant thrust), PAX (Paxton thrust), GUN (Gunnison thrust), SDD (Sevier Desert detachment fault).

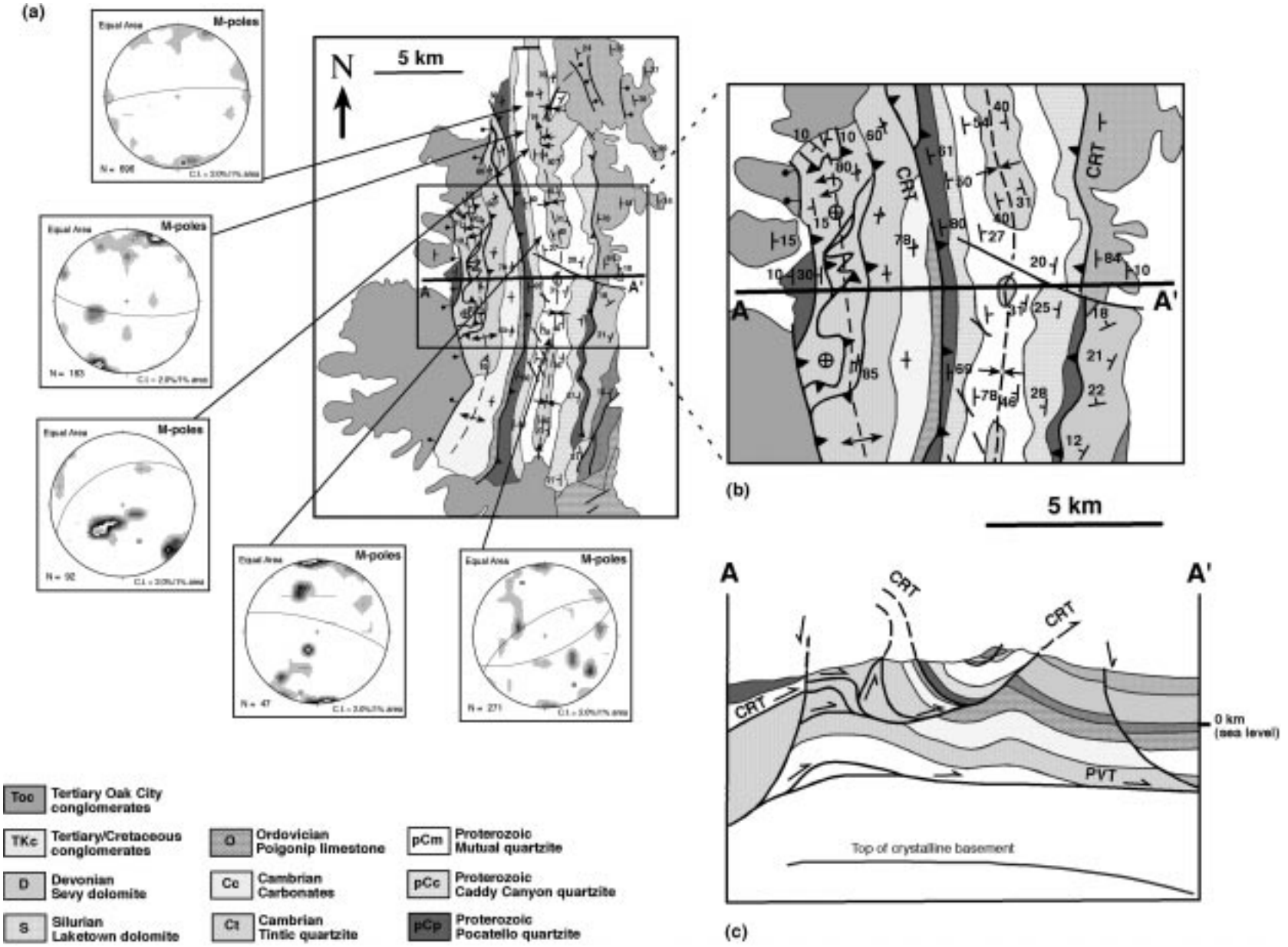

Fig. 2. (a) Geologic map of the Canyon Range showing first order faults and folds and equal-area plots of poles to M-planes throughout the Canyon Range (CR) syncline. The best fit great circles illustrate the average cumulative E–W motion plane for the CR syncline. (b) Enlarged map view from boxed area in part (a). Line of regional cross section (AA') is shown in both map views. (c) Cross-section AA′ showing the folded Canyon Range thrust and the sub-thrust duplex.

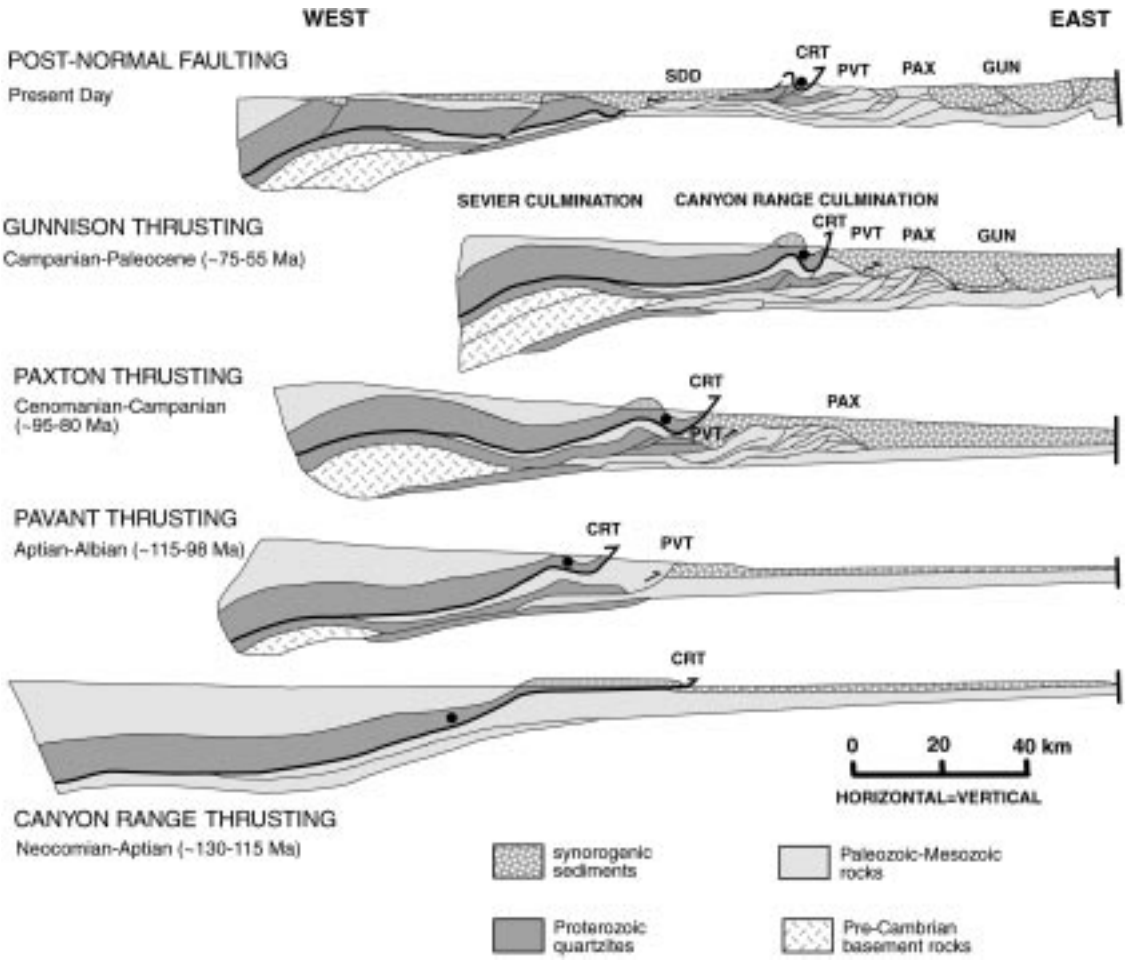

Fig. 3. Kinematic history of the central Utah segment of the Sevier FTB with incrementally restored regional cross-sections showing the approximate shapes of the orogenic wedge during emplacement of successive major thrust sheets in the Canyon Range. Black dots indicate location of the rocks studied through time. The Canyon Range thrust (CRT), Pavant thrust (PVT), Paxton thrust (PAX), Gunnison thrust (GUN) and the Sevier Desert Detachment (SDD), a low angle normal fault, are shown.

Step-wise unfolding of the tightest part of the syncline using angular unconformities between conglomerate units, which are present on both limbs of the fold, indicates that at the time of first conglomerate deposition, the fold interlimb angle was 156°, and that erosion reached the level of the Cambrian rocks (Mitra and Sussman, 1997). Successive stages in the unfolding history suggest that progressive fold tightening took place mainly by rotation of the west limb to a present-day interlimb angle of 33°.

Based on the overprinting of structures and the unfolding history of the tightest part of the fold, we interpret the along-strike variations in geometry, i.e. tightness, thickness variation of beds and hinge shape of the fold, as equivalents of temporal stages in fold growth. Thus, variations in cross-sectional geometry along the length of the fold represent snapshots of its folding history (Fig. 4). These variations result from differences in the number, size and behavior of fault slices in the duplex in the core of the adjoining anticline.

2.3. Variation in fold geometry due to fold tightening

The CR syncline is composed of thick-bedded quartzite units with a small material contrast between layers, limiting the role of flexural slip during fold growth and tightening (Bayly, 1974). In a very tight fold with thick and constant bed thickness, a space problem often develops within the fold core, which may be relieved by a discontinuity, such as an out-of-the-core thrust (Price, 1967). However, most tightening in the CR syncline was accomplished by rotation of one limb accompanied by limb thinning, and possible hinge migration (Mitra and Sussman, 1997). The limb progressively thinned and rotated towards the overall transport direction of the CRT sheet (Mitra and Sussman, 1997). Some evidence for hinge migration is seen as an increase in outcrop-scale fracture density in regions where we would expect hinge migration based on the kinematic model of Mitra and Sussman (1997).

The thickness and geometry of the limbs and hinge are based on a series of down-plunge projections and

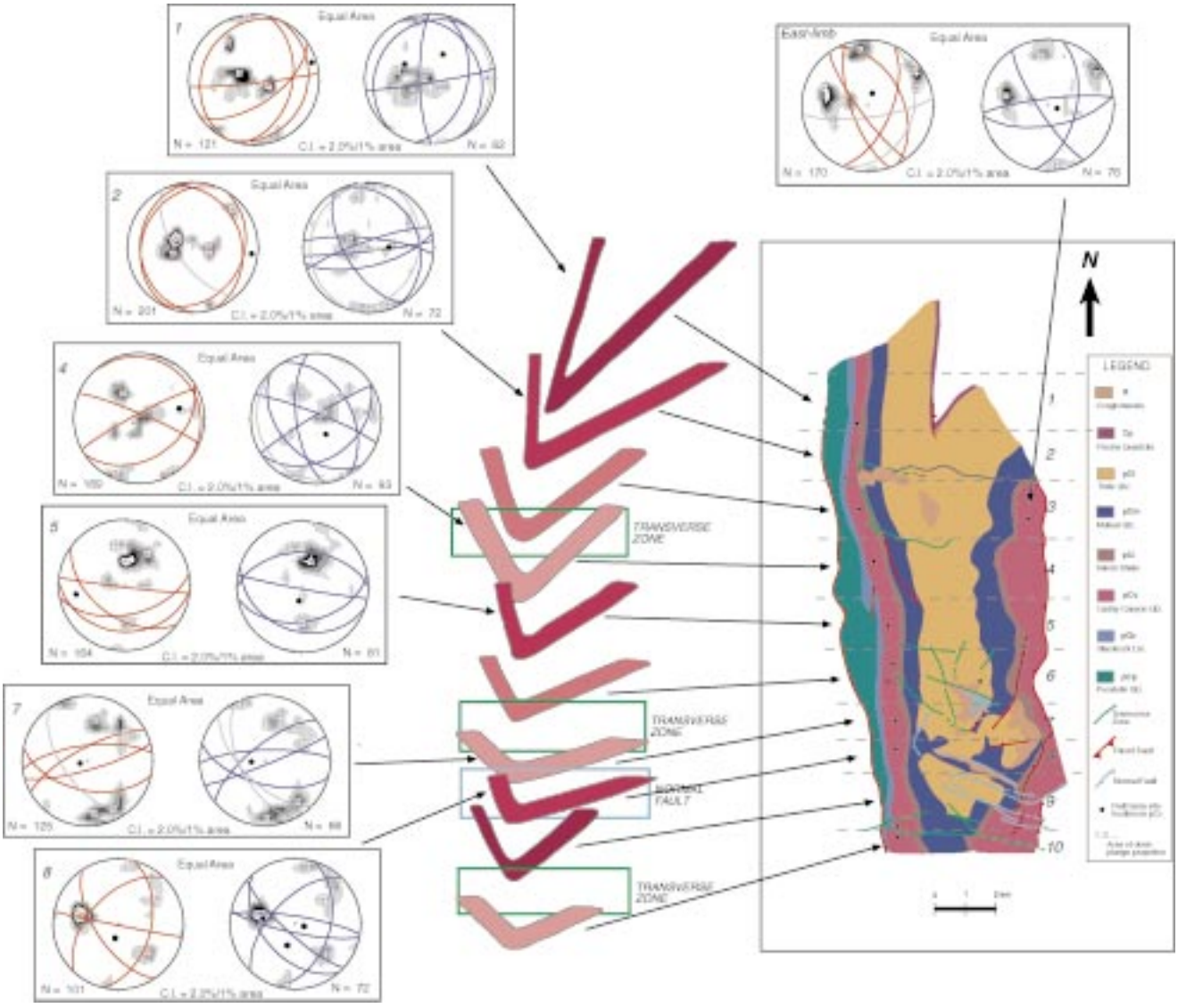

Fig. 4. Map and cross-sections of Canyon Range syncline. Ten fold profiles show only the Proterozoic Caddy Canyon Quartzite. Bed thickness for the 10-fold profiles are directly comparable: 3, 7, 8 and 10 did not significantly thicken or thin during folding. Darker colors represent areas where the fold underwent relatively more complex and prolonged deformation. The fracture arrays for the west limb and one representative site on the east limb of the Canyon Range syncline are shown as pairs of stereograms showing the "true" plot and the "orientation" plot. Red lines (and their pink poles) indicate the conjugate-conjugate fractures used in the "true" plots while the blue lines (and their light blue poles) indicate the conjugate-conjugate fracture sets used in the "orientation" plots to determine the maximum shortening directions (black dots). The determined shortening directions for area 7 are similar in both the "true" and "orientation" plots, due to the influence of the steep normal faults at the southern end of the range.

cross-sections constructed along the length of the CR syncline. The CR syncline is divided along its length into 10 different down-plunge projection areas according to variations in fold geometry (Fig. 4, Table 1). Although the overall fold shape changes from an open fold at its southern end to a tight, overturned fold at its northern end, in detail the variation is not laterally continuous because the fold is cut by transverse zones across which there are abrupt fold geometry changes. Therefore, the 10 areas are grouped into four transverse-zone-bound-segments. Areas 1, 2 and 3 are in the northern-most segment; areas 4, 5 and 6 in the central segment; areas 7, 8 and 9 in the southern segment; and area 10 in the southernmost segment. Since fold geometry changes significantly across the three transverse zones, we infer that folding history within each segment is unique (Fig. 4, Table 1).

3. Fracture networks

3.1. Data collection

A total of 63 locations (sites) along the west limb and several transects across the CR syncline were selected to examine fracture network variation with position, hinge surface attitude, fold plunge and fold tightness. The east

Table 1
Fold geometry summary of the 10 down-plunge areas (compare with Fig. 4)

Down-plunge area	Interlimb angle (°)	West limb dip (°) (from down-plunge projection)	~ % of thinning (-) or thickening (+) of west limb
1	31	75 (overturned)	−40
2	60	90	−33
3	72	70	0
	transverse zone		
4	79	57	+23
5	73	75	−9
6	94	60	−5
	transverse zone		
7	128	35	0
8	99	60	0
9	80	60	−20
	transverse zone		
10	114	35	0

limb of the syncline underwent little or no rotation and has very few fractures. We infer that the fracture patterns on the east limb (Fig. 4) represent deformation that took place during the early stages of folding and use them as a reference frame to interpret the fracture patterns in the west limb. In this paper, we focus on 10 of the 63 stations (black dots on maps on Figs. 4 and 10) on the west limb of the fold in the Proterozoic Caddy Canyon quartzite, a nearly homogeneous, coarse-grained orthoquartzite. This unit has thick (1–5 m), massive beds and lacks material heterogeneities that may influence the development of fracture patterns. Sampling locations range from 1.4 km to 1.6 km from the hinge region of the syncline and from 0.7 km to 1.2 km of the Canyon Range thrust (Fig. 4). Therefore, overprinting fracture patterns due to localized deformation within the hinge region and close to the damage zone of the CRT are avoided. Each site is representative of the west limb for each area.

To understand the bulk behavior of fractured rocks, detailed quantitative measurement of the deformation is required (Figs. 4 and 5). At each location, detailed sketches of fracture geometry were made and morphological descriptions recorded using 1 m^2 grids (subdivided into 10 cm squares) on two mutually perpendicular surfaces to obtain the three-dimensional geometry of the fracture network. From these fracture sketches and descriptions, we constructed slip-linear plots, determined M-plane orientations (Angelier, 1979), defined overall shortening directions, and determined the most common slip surfaces at each location. We then compared the data sets to infer the evolution of the local fracture populations, which in turn were used to infer folding history.

3.2. Fracture stages

Fracture populations that developed during folding of the CR syncline form a deformation fabric that is penetrative at the outcrop scale (Fig. 5). In the simple case, the formation of a single fracture or a set of fractures is an instantaneous process related to the active stress field and principal stress directions can be determined from the fracture orientation. However, because of material anisotropies in the rocks and anisotropies in stress created by the fractures themselves, it is impossible to define a unique stress tensor for a group of fractures in a rock (Arthaud, 1969). In addition, for an evolving fold such as the CR syncline, later deformation occurs along pre-existing fractures and/or new fractures form during successive stages of fold tightening. Therefore, the observed fracture patterns are cumulative. Thus, the collective character of the fracture population (Fig. 4) reflects overall deformation more accurately than individual fractures, and provides shortening directions rather than maximum compressive stress directions (e.g. Arthaud, 1969) for each stage of folding. Consequently, we have attempted to determine shortening directions rather than stress orientations for separate stages of fold tightening along the fold.

Successive generations of fractures were distinguished on the basis of their microscopic (Sussman, 1995) and their mesoscopic (this study) characteristics, cross-cutting relationships and degree of reactivation. Recrystallized fractures and zones observed at the outcrop scale are the oldest features and probably formed while the rocks of the CR sheet were at depth (Fig. 5). Mutually cross-cutting relationships with thrust-related cleavage at the microscopic scale (Sussman, 1995) are interpreted to suggest that these fractures and zones formed during initial emplacement of the CRT sheet, and may be the result of motion of the sheet over ramps. Features developed during the later stages of folding and fold tightening include: open and shear fractures, breccia zones, cataclasite zones, stylolites, and cemented and healed zones (Fig. 5e). The oldest features are the healed zones (with and without iron oxide staining) and are cross cut by unhealed fractures and zones (Fig. 5e). If insufficient cross cutting information was available, we assumed that the most prominent and reactivated zones were the youngest.

The tighter areas of the CR syncline do not necessarily imply that the folding in those areas began earlier or continued later than the more open fold profile areas. However, we assume that the tightest areas of the CR syncline, as seen at the northern end of the range, went through early folding geometries now represented by the more openly folded areas to the south. Therefore, we might expect that by removing successive stages of fracturing from the tighter fold profiles, we should find similar fracture patterns to those preserved in the more open fold profiles. However, such a "stackability" of fracture stages is not found because: (1) later deformation during folding may reactivate existing fractures rather than forming new ones; and (2) deformation to create the same incremental change of folding geometry occurred at different times and perhaps different conditions in different segments. Variations in fracture network patterns at different places on the fold indicate differences

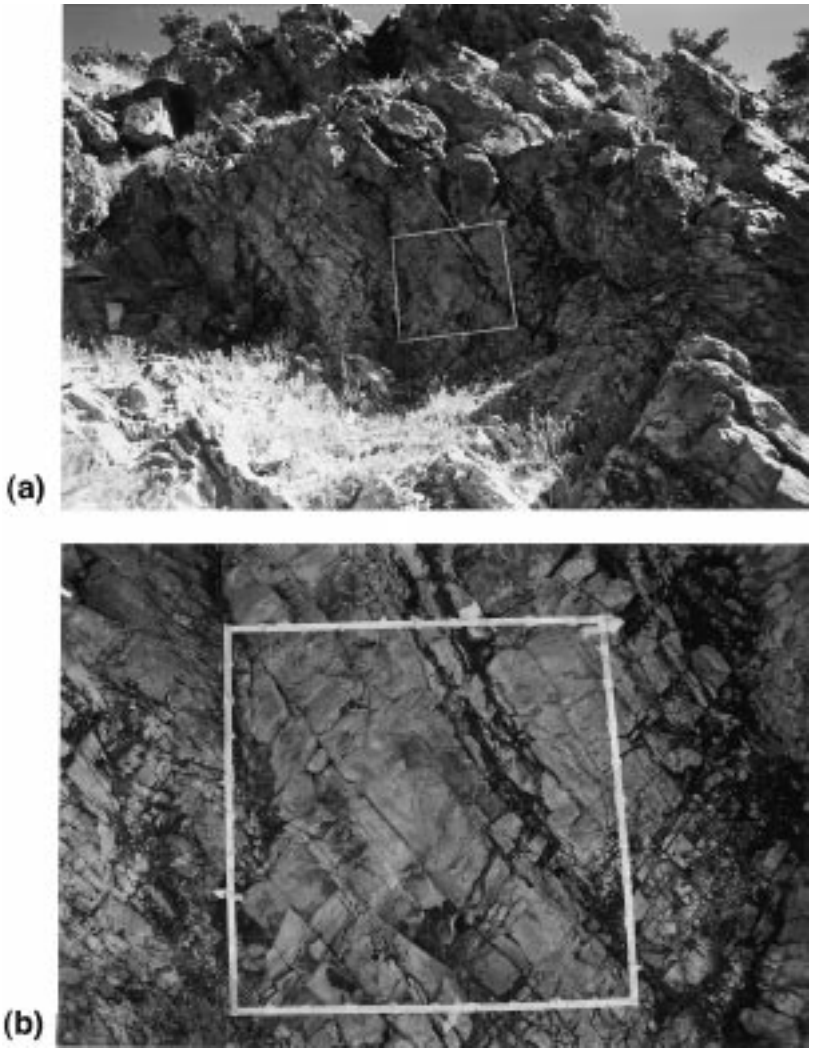

Fig. 5. (a–e) Mesoscale fracture patterns from area 9. (a) Outcrop of Proterozoic Caddy Canyon quartzites of the Canyon Range syncline showing homogeneous fracturing at the outcrop scale. (b) Typical fracture sets seen in the outcrop (1 m × 1 m grid for scale). (c) Detailed field sketch of the fracture patterns within the 1 m × 1 m grid. (d) Sketch (c) with mesoscale blocks highlighted and six lines of transect used for Spektor chord analysis (Underwood, 1970). (e) Close up photo showing outcrop scale deformation features: recrystallized zones (R), healed zones (H), open fractures (OF), breccia zones (B), cataclasite zones (C), stylolites (STY). The latest stage features (LDZ) in this area are parallel to bedding (double headed arrow). Bedding heterogeneities often influence fracture development and maintain bed parallel slip, although to a lesser degree, during later stages of fold tightening. Note that bedding is still preserved, even though a significant amount of deformation has taken place in area 9.

in deformation history (Fig. 4) and each area must be analyzed independently.

3.3. Fracture sets

Coulomb theory describes the relationship between stress and shear fractures produced in a confined compressional setting and predicts that fractures form in a conjugate set bisected by the maximum compressive stress, yielding plane strain. Naturally deformed materials, however, often show at least two pairs of conjugate sets of fractures. Reches (1978) emphasized that in a three-dimensional strain field at least two pairs of conjugate fractures form arranged in orthorhombic symmetry. The acute bisectrix of the conjugate–conjugate fracture sets provides the shortening direction (and maximum compressive stress direction).

Assuming three-dimensional strain, fracture populations from each station were examined to find conjugate–conjugate fracture sets to determine shortening direction(s) for a stage of folding (black dots in stereograms in Fig. 4) (Reches, 1983). Conjugate–conjugate fracture sets were identified in the field on the basis of: cross-cutting relationships, morphology and development of fractures.

Grid locations were carefully selected to most accurately represent fracture and deformation zone population in a given area. For each site, we show two different stereograms based on the collected fracture population data (Fig. 4). In both types of stereograms, the orientations of fractures sets were derived from clustering of fractures poles and shown as

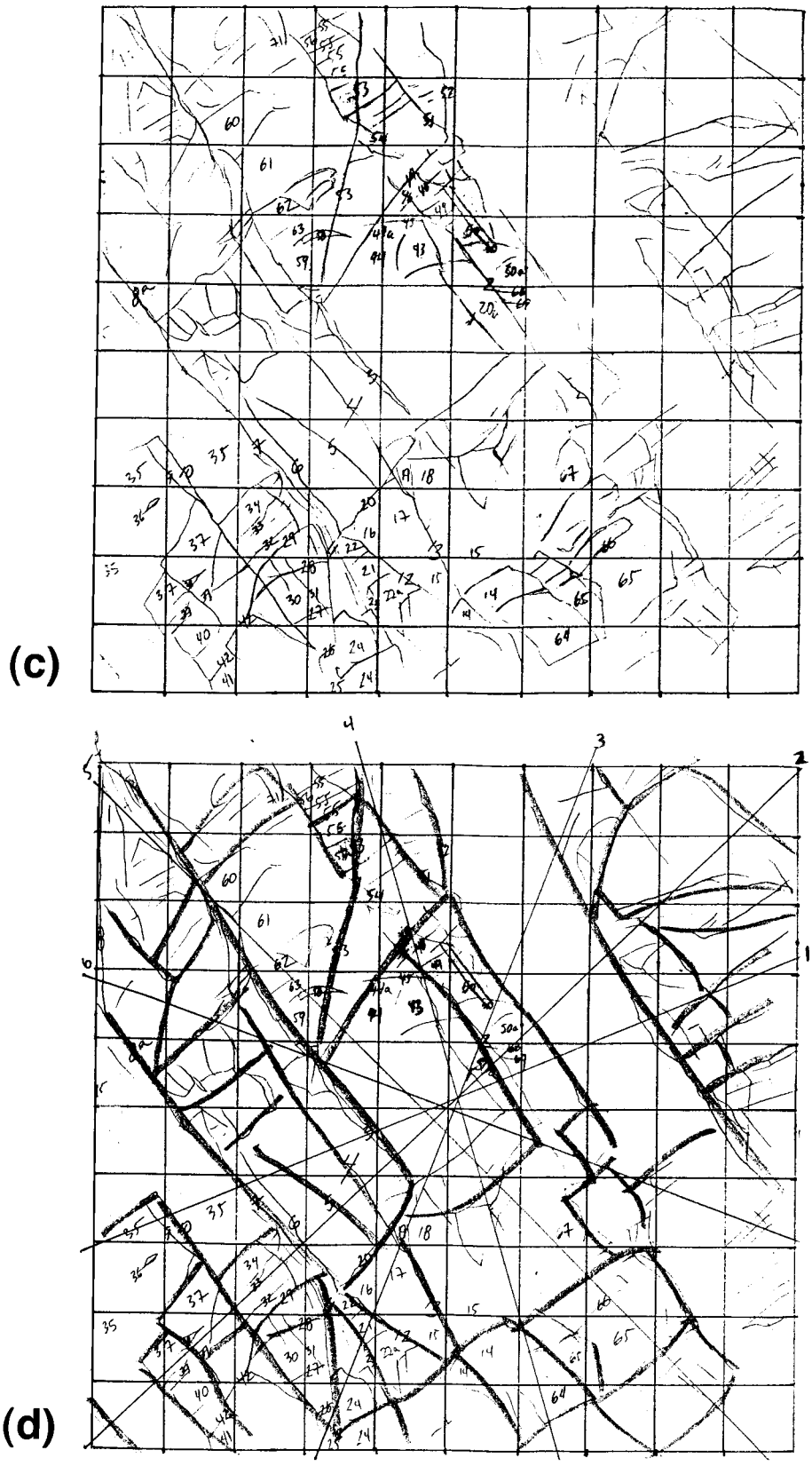

Fig. 5. (*continued*)

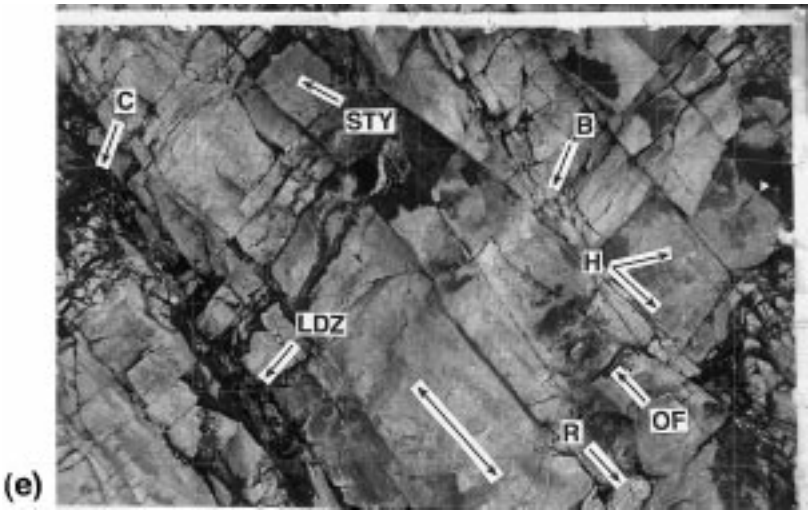

Fig. 5. (*continued*)

great circles. In each case, the stereogram on the left shows every recognizable fracture within a site location, resulting in the most prominent (i.e. continuous fractures and thick deformation zones showing reactivation and well developed breccia or cataclasite) fracture sets being weighted most heavily. We refer to these stereograms as the "true" plots (Fig. 4). The second stereogram is an "orientation" plot in which each *fracture set* is given equal importance. In other words, if there were *n* fractures with the same orientation and character, they would plot as one point on the "orientation" plot.

Since the most recently formed fractures in any area are usually the most prominently developed, the "true" plot can be used to evaluate the latest stage of fracturing at a site. The great circles used in the "true" plots were those based on the highest pole percentage. The "orientation" plot, on the other hand, exposes relict fracture patterns (such as healed and poorly developed fractures) that may be hidden by the dominant fracture sets formed during the latest stage at a given site (Figs. 4 and 5). The great circles used to determine the conjugate–conjugate sets used each pole concentration equally. The shortening directions remained consistent even in cases where there were multiple conjugate–conjugate sets (e.g. Fig. 4, Area 4).

Assuming along strike variations in fold geometry can be correlated with temporal changes during fold growth, the last fractures in a particular geometry were the active fractures in a particular folding stage. The "true" plots with their bias to the youngest, more abundant fractures, are the better tool for identifying these features in each area. The results of the different "true" plots may be compared to describe changes in fracture patterns during fold tightening and a complete kinematic history can be obtained (Figs. 4 and 5).

To compare the deformation patterns from adjoining areas, the "true" plot from one area is stereographically manipulated to reflect the fold geometry (tightness) and orientation (plunge) of the adjoining area (Fig. 6a,b, Table 2). The comparisons differ more across segment boundaries than within segments (Fig. 6a,b, Table 2). For example, areas 1 and 2 are both within the northern-most segment; when the "true" plot from area 1 is unfolded to the degree of folding in area 2, the unfolded shortening direction is comparable to that seen in area 2 (Fig. 6a). Areas 2 and 4, on the other hand, are separated from one another by a transverse zone (Fig. 4), and shortening directions for 2 when unfolded to 4 do not match (Fig. 6b).

Along the entire length of the fold, the acute bisectrix of the conjugate–conjugate fracture sets on the "orientation plots" is generally steep, suggesting an approximately up/down shortening direction (Fig. 4, Table 3). The fractures defining this shortening direction are generally healed and/or poorly developed; thus, they probably developed during the early stages of folding. The earliest fractures could have formed when the beds were horizontal or gently dipping. In the simplest case of horizontal beds, following Andersonian fault theory (Anderson, 1951), the fractures formed would have had dips of ~30°E or W. In a more complex, natural system, conjugate–conjugate fracture sets would form with low dips. We infer that these fractures were rotated with bedding as the west limb of the CR syncline rotated during fold tightening, so that their present orientations indicate "steep" shortening directions which are slightly variable because all areas may not have started fracturing at the same fold geometry (Table 4).

The observed fracture sets on the "orientation" plots from different locations have been placed within a temporal context by incremental unplunging and unfolding of the limbs of the syncline from each transverse zone bounded domain. For comparing the deformation in two adjoining areas the "orientation" plots from each are stereographically manipulated to reflect the fold geometry (tightness) and orientation (plunge) of the adjoining area (an example is shown in Fig. 7a,b, Table 3). We lack sufficient control

"True" plot stereographic manipulations

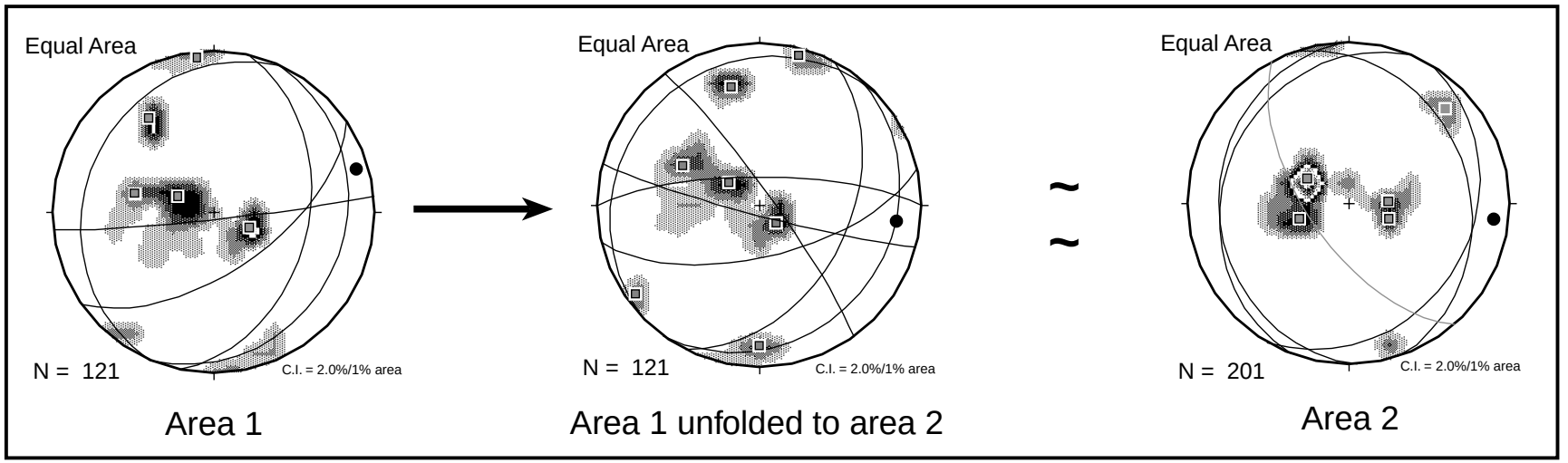

(a)

N = 201

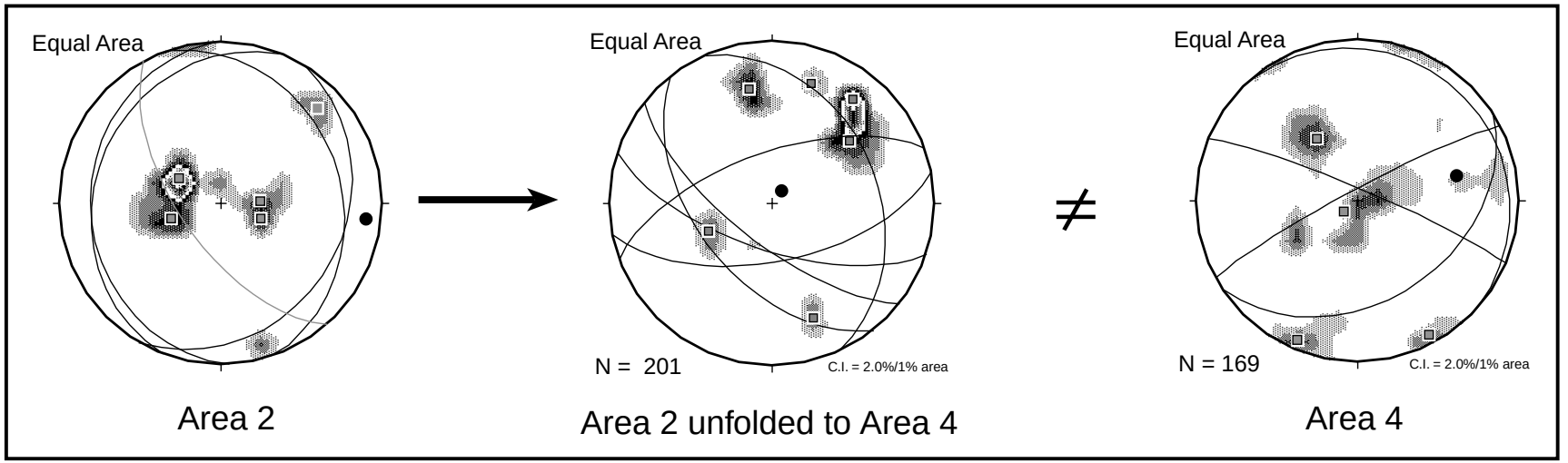

(b)

Table 2
"True" plot stereographic manipulations (compare with Fig. 6)

Two areas being compared	Amount of plunge removal (plunge, trend)	Areas' bedding orientations for amount of dip removal (dip, dip direction)	Shortening direction before rotation (plunge, trend)	Shortening direction after rotation (plunge, trend)		Shortening direction compared to (plunge, trend)
Area 1 unfolded to Area 2	(17,357)	Area 1: (75, 278) Area 2: (85, 100)	Area 1: (22,077)	Area 1 → Area 2: (30,096)	≈	Area 2: (12,094)
Area 2 unfolded to Area 3	(16,352)	Area 2: (85, 100) Area 3: (70, 080)	Area 2: (12,094)	Area 2 → Area 3: (66,028)	≈	Area 3: (68, 060)
Area 3 unfolded to Area 4 (across a transverse zone)	(16,350)	Area 3: (70, 080) Area 4: (47, 074)	Area 3: (68,060)	Area 3 → Area 4: (88,050)	≠	Area 4: (35,078)
Area 4 unfolded to Area 5 &	(15,350)	Area 4: (47, 074)	Area 4: (35,078)	Area 4 → Area 5: (28,232)	≈	Area 5: (23,260)
Area 5 unfolded to Area 4		Area 5: (70, 076)	Area 5: (23,260)	Area 5 → Area 4: (30,250)	≠	Area 4: (35,078)
(The dominant folding mechanism is different for Areas 4 and 5. A space problem is relieved from the core of the fold in Area 4 with an out of the core thrust during fold tightening while area 5 continues to fold tighten by limb thinning and limb rotation. Therefore, the two areas cannot be compared. Note: Area 5 is also unfolded to Area 4 because Area 5 has a tighter fold geometry.)						
Area 5 unfolded to Area 6	(10,352)	Area 5: (70, 076) Area 6: (55, 080)	Area 5: (23,260)	Area 5 → Area 6: (80,229)	≈	Area 6: (85,227)
Area 6 unfolded to Area 7 (across a transverse zone)	(5,355)	Area 6: (55, 080) Area 7: (48, 081)	Area 6: (85,227)	Area 6 → Area 7: (75,100)	≠	Area 7: (82,257)
Area 7 unfolded to Area 8 &	(2,011)	Area 7: (48, 081)	Area 7: (82,257)	Area 7 → Area 8: (68,271)	≠	Area 8: (81,070)
Area 8 unfolded to Area 7		Area 8: (60, 080)	Area 8: (81,070)	Area 8 → Area 7: (73,247)	≠	Area 7: (82,257)
(Areas 7 and 8 are separated by a large normal fault system, so the continuity in their folding mechanisms may be affected. Therefore, Areas 7 and 8 may not have a strong correlation. Note: Area 8 is also unfolded to Area 7 because Area 8 has a tighter fold geometry.)						
Area 8 unfolded to Area 9	(1,017)	Area 8: (60, 080) Area 9: (60, 080)	Area 8: (81,070)	Area 8 → Area 9: (76,156)	≈	Area 9: (75,212)
Area 9 unfolded to Area 10 (across a transverse zone)	(2,011)	Area 9: (60, 80) Area 10: (50, 090)	Area 9: (75,212)	Area 9 → Area 10: (52,220)	≠	Area 10: (89,143)

for detailed retrodeformation steps for unplunging and unfolding the "orientation" plots. We have used end case approaches in each area: (1) completely unfold and then completely unplunge or (2) completely unplunge and then completely unfold. Both approaches were applied to each down plunge area and produced very similar results (Fig. 7a,b, Table 3). In each case, the shortening direction remains consistent, indicating that the CR syncline initially folded in a very similar manner along strike.

3.4. Motion planes and slip linear plots

For a single sliding surface, a motion plane (M-plane) contains the slickenline orientation and the pole to the slickenside surface, i.e. the fault surface. For a population of sliding surfaces formed at the same stage of deformation, a clustering of poles to M-planes defines the overall M-plane orientation. The overall M-plane orientation, which defines the plane of tectonic transport, is consistently E–W subvertical throughout the deformation (Fig. 2) and remained approximately constant throughout the fold. However, this includes lineation data from all fractures, many of which were older features. Therefore, M-plane analysis was applied to data for the youngest fractures identified from "true" plots; M-planes for these active fractures intersect with the fracture poles of the "true" plots (see Fig. 8). Their associated slip linears (Fig. 8e), along with field observations, were used to describe the relative motion of the mesoscale fault-bound blocks during folding (as described in Section 4.3).

3.5. Mesoscopic block sizes

The fracture networks break up the rock into blocks of a variety of sizes. The size distribution of blocks can be determined using Spektor chord analysis (Underwood, 1970) by measuring fracture spacing on randomly oriented traverses across the detailed outcrop sketches (Fig. 5d). Assuming equidimensional blocks, the average block size ranges from 0.15 to 0.23 m.

Fig. 6. "True plots" in which the fold geometry (interlimb angle) and the orientation (plunge and trend) are stereographically manipulated to match those of an adjoining area. Areas 1 and 2 are within one transverse-zone-bound-segment while Areas 2 and 4 are in two different transverse-zone-bound-segments. Conjugate-conjugate fracture sets provide the maximum shortening direction (black dots). (a) Area 1 unfolded to Area 2. (b) Area 2 unfolded to Area 4. (Area 2 is representative of the northern-most segment. See Table 2 for further details.)

Table 3
"Orientation" plot stereographic manipulations (compare with Fig. 7)

Two areas being compared	Areas' bedding orientations for amount of dip removal (dip, dip direction)	Amount of plunge removal (plunge, trend)	Shortening direction before rotation (plunge, trend)	Shortening direction after rotation: unfolded then plunge removed (plunge, trend)	Shortening direction after rotation: plunge removed then unfolded (plunge, trend)	Shortening direction compared to (plunge, trend)
Area 1 unfolded to Area 2	Area 1: (75, 278) Area 2: (85, 100)	(17,357)	Area 1: (61,318)	Area 1 → Area 2: (79,104)	Area 1 → Area 2: (68,087)	Area 2: (68,089)
Area 2 unfolded to Area 3	Area 2: (85, 100) Area 3: (70, 080)	(16,352)	Area 2: (68,089)	Area 2 → Area 3: (73,080)	Area 2 → Area 3: (75,071)	Area 3: (75,072)
Area 3 unfolded to Area 4 (across a transverse zone)	Area 3: (70, 080) Area 4: (47, 074)	(16,350)	Area 3: (75,072)	Area 3 → Area 4: (69,128)	Area 3 → Area 4: (60,160)	Area 4: (71,148)
Area 4 unfolded to Area 5 & Area 5 unfolded to Area 4	Area 4: (47, 074) Area 5: (70, 076)	(15,350)	Area 4: (71,148) Area 5: (76,193)	Area 4 → Area 5: (72,199) Area 5 → Area 4: (80,214)	Area 4 → Area 5: (74,150) Area 5 → Area 4: (74,290)	Area 5: (76,193) Area 4: (73,148)
(Rotated orientation plots of Areas 4 and 5 have consistent results (i.e. steep plunge), indication that a change in folding mechanism occurred during later fold tightening stages. Note: Area 5 is also unfolded to Area 4 because Area 5 has a tighter fold geometry).						
Area 5 unfolded to Area 6	Area 5: (70, 076) Area 6: (55, 080)	(10,352)	Area 5: (76,193)	Area 5 → Area 6: (85,060)	Area 5 → Area 6: (81,077)	Area 6: (88,087)
Area 6 unfolded to Area 7 (across a transverse zone)	Area 6: (55, 080) Area 7: (48, 081)	(5,355)	Area 6: (88,087)	Area 6 → Area 7: (78,094)	Area 6 → Area 7: (85,062)	Area 7: (81,265)
Area 7 unfolded to Area 8 & Area 8 unfolded to Area 7	Area 7: (55, 080) Area 8: (48, 081)	(2,011)	Area 7: (88,087) Area 8: (81,265)	Area 7 → Area 8: (78,094) Area 8 → Area 7: (80,301)	Area 7 → Area 8: (85,062) Area 8 → Area 7: (84,039)	Area 8: (81, 265) Area 7 (88,087)
(Rotated orientation plots of Areas 7 and 8 have consistent results (i.e. steep plunge), indication that the large normal fault system is active during later stages of fold tightening. Note: Area 8 is also unfolded to Area 7 because Area 8 has a tighter fold geometry).						
Area 8 unfolded to Area 9	Area 8: (60, 080) Area 9: (60, 080)	(1,017)	Area 8: (84,62)	Area 8 → Area 9: (79,089)	Area 8 → Area 9: (83,070)	Area 9: (85,104)
Area 9 unfolded to Area 10 (across a transverse zone)	Area 9: (60, 080) Area 10: (50, 090)	(2,011)	Area 9: (85,104)	Area 9 → Area 10: (83,051)	Area 9 → Area 10: (86,040)	Area 10: (84,020)

Table 4
Each of the 10 areas' present shortening directions compared to their de-plunged and unfolded shortening directions[a]

Down-plunge area	Shortening direction (plunge, trend)	Amount of plunge removed (plunge, trend)	Amount of bedding dip removed (dip, dip dir.)	De-plunged and unfolded shortening direction (plung, trend)
1	(53,303)	(19,358)	(78,278)	(30,348)
2	(60,082)	(16,355)	(85,100)	(10,245)
3 west limb	(75,257)	(16,350)	(70,080)	(10,260)
3 east limb	(80,093)	(16,350)	(36,298)	(04,311)
4	(72,136)	(16,350)	(47,074)	(10,084)
5	(77,205)	(15,350)	(70,076)	(39,295)
6	(88,198)	(05,355)	(55,080)	(07,057)
7	(67,277)	(05,355)	(48,081)	(08,107)
8	(83,094)	(00,017)	(60,080)	(36,280)
9	(82,102)	(00,017)	(60,080)	(12,229)
10	(85,336)	(02,185)	(50,090)	(27,088)

[a] Note: shortening direction trends from de-plunged and unfolded areas that are not E–W (e.g. Area 1) may be due to local variations in early deformation.

4. Kinematics of folding

4.1. Model for fracturing during fold tightening

If rocks are folded, the deformation is inhomogeneous (Ramsay, 1967) and the fracture populations (formed at an instant during folding) vary from the limbs to the hinge of the fold (Price, 1967; Hancock, 1985). For a fold undergoing progressive tightening by limb rotation under constant horizontal shortening, a complex population of fractures should develop at any location within the fold. A simple model, assuming plane strain folding, is used to illustrate the pattern of development of fractures and their behavior during progressive fold tightening (Fig. 9a). The model provides a start to unraveling the complex fracture patterns observed in the CR syncline.

The model starts with a horizontal bed with bed-parallel compression. Conjugate sets of shear fractures form with the maximum compressive stress orientation as the acute bisector, along with extension fractures parallel to the maximum compressive stress direction. As the fold tightens, the orientation of the fold limbs with respect to the maximum compressive stress direction progressively changes, and a new set of conjugate and extension fractures form. Earlier formed fractures that remain in convenient orientations for sliding or extension remain active. Original shear fractures may evolve into extension fractures, and vice versa. At any particular stage of deformation, active shearing fractures lie $30 \pm 20^\circ$ from the maximum compression direction, while actively extending fractures lie at $<10^\circ$ from the maximum compression direction (Bles and Feuga, 1986; Twiss and Moores, 1992). Fractures undergoing healing under compression and/or stylolite formation lie at angles of 80–90° from the maximum compression direction, and inactive fractures lie at angles of 50–80° from the maximum compression direction.

The model shows folding of both limbs to an interlimb angle of 100° (i.e., 40° limb dips), with continued fold tightening taking place by rotation of one limb. The rotating limb would then have a higher density of fractures. This simple, plane strain model is similar to the folding history of the CR syncline with a constant overall E–W vertical motion plane (Fig. 2), and where the east limb reached a constant maximum dip of no more than 40–50° while the west limb continued to be rotated to vertical and overturned dips as the fold tightened.

Additional complexities (not shown) to this simple model result as different sets of fractures form within the hinge region (due to local variations in the stress field there). Hinge zone fractures migrate into the rotating limb if there is hinge migration, and overprinting fractures form near transverse zones. Also, in a three-dimensional strain field the shear fractures form in conjugate–conjugate sets with an orthorhombic symmetry (Fig. 9b, Reches 1978; Reches and Dieterich, 1983). These additional complexities allow us to explain the details of the patterns of fracture populations observed in the CR syncline.

Multiple overprinting fracture sets, at the outcrop scale, eventually form a system of fracture bounded blocks of vastly different sizes. Different size classes may be organized into subsystems (Fig. 9a). Movement along the fractures would result in gaps and overlaps between the moving blocks, leading to further fracturing and smaller blocks to maintain continuity between larger size classes. Progressive development and organization of subsystems continues with increasing deformation forming the blocks with the most energy efficient shapes (i.e. the most space filling). With enough size classes formed, the material behaves in a ductile manner and flows by mesoscopic cataclastic flow. Such flow involves fracturing, loss of cohesion and frictional sliding at all scales due to a dispersed, interconnected network of fractures.

4.2. Variation of fracture-network pattern relative to position on the fold

Different fold tightening mechanisms are dominant in successive down plunge areas. For example, in areas 1, 2,

"Orientation" plot stereographic manipulations

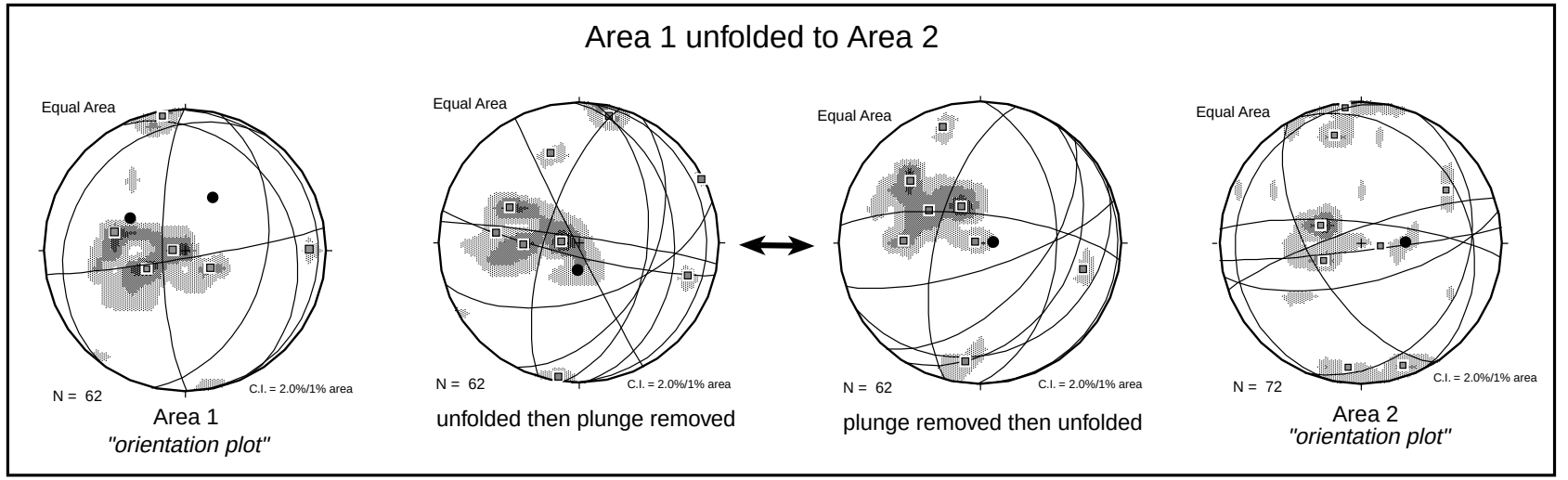

(a)

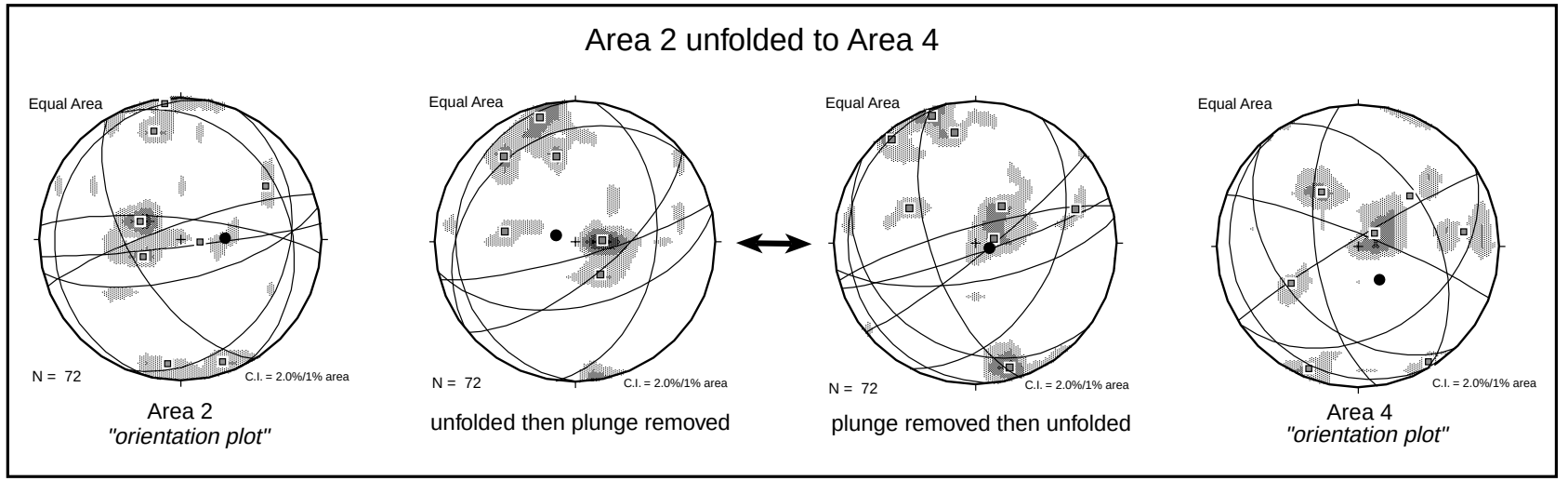

(b)

8 and 9 (Fig. 4) the fold remains continuous and tightening is accommodated by varying degrees of limb thinning accompanied by possible hinge migration, while in area 4 fold tightening is accommodated by out of the core thrusting (Fig. 4). Variations of fracture-network patterns would presumably result from differences in deformation history in different parts of the fold. The fracture patterns represent many superposed increments of fracturing during fold growth. Therefore, the geometric and kinematic relationship of fracture network evolution and fold growth under shallow crustal conditions can only be successfully determined by separating successive generations of fractures on the basis of cross-cutting relationships, fracture character and orientation, and degrees of reactivation.

Microstructural studies of deformation zones (DZs) are useful for this analysis because relict deformation phases are well preserved as recataclasized zones. For example, the CR syncline has undergone a very complex and prolonged history of folding in area 2, which has an interlimb angle of 60° (Fig. 4). At least two stages of cataclastic flow are observed at the microscale from this area, which is the largest number of cataclastic events seen at this scale within the CR syncline (similar to Fig. 10a). The CR syncline has an interlimb angle of 80° in area 4 and only one stage of cataclastic flow is observed at the microscale. In areas of greater interlimb angles (e.g. area 7 with an interlimb angle of 124°), no DZs are observed at the microscale (Fig. 10b). In addition, because cataclastic flow generally results in dilatancy, fluid pressure within the cataclasite zones fluctuated considerably during reactivations. This change is indicated at the microscale by successive series and recataclasis of iron oxide precipitate from multiple generations of fluid flow and dispersed fracture formation (Fig. 10a) (Twiss and Unruh, 1998). Similar patterns are observed with the mesoscopic fracture networks, which are best developed in areas 2 and 9 (Fig. 5).

We may expect to find fractures that are reactivated as deformation zones in addition to new fractures in regions where the CR fold has the smallest interlimb angle; i.e., where there is the most limb rotation. As folding progresses, the earlier fractures formed may be reactivated as deformation zones, if they continue to be in convenient orientations. This reactivation would result in reduction in grain size within the DZs bounding the mesoscale blocks. Multiple stages of reactivation on previously formed zones may result in large outcrop scale block sizes. Alternatively, earlier formed fractures may rotate to inappropriate orientations and become mechanically hardened, resulting in more fracturing at the next stage of deformation. This would result in an overall reduction in the size of mesoscopic blocks bounded by fractures and DZs with minimal amounts of reactivation.

4.3. Large-scale strain by cataclastic flow

The scale of fractures in the CR syncline range from micro-scale cracks to map-scale transverse zones. We have focused on mesoscale fractures whose distribution is approximately homogeneous at the scale of the outcrop (Wojtal, 1989). If deformation is accommodated by a large number of slip events on many fractures and DZs, and the deformation scale is large compared to the size of the fractures and DZs on which deformation is accommodated, then the resultant deformation may be approximated as homogeneous and continuous (Twiss and Unruh, 1998). In the CR syncline, the motion on individual fractures and DZs bounding the outcrop-scale blocks is very small compared to the overall deformation of the beds in the CR syncline, as evidenced by the preservation of bedding from block to block (Fig. 5). Clearly, motion along the DZs do not need to be large to accommodate very tight folding (Hadizadeh and Rutter, 1983). Contrasting mesofracture assemblages in different parts of the fold (Fig. 4) reflect different bulk strain histories and can be used to constrain the motion of the beds containing those fractures.

On a regional scale, the Caddy Canyon Quartzite shows uniform thickness (~585 m) along the length of the Canyon Range (Holladay, 1983), and this thickness is typically observed in the little-deformed east limb of the CR syncline (Fig. 4, Table 1). The overall strain during fold tightening is measured by the thinning or thickening of the Caddy Canyon Quartzite at the map scale, which can be estimated from down-plunge projections, assuming plane strain (Fig. 4). The thinning and thickening is accomplished dominantly by the "jostling" motion of large blocks, bounded by mesoscale DZs, during fold tightening. Unfortunately, the lack of good offset markers across faults prevents direct measurement of the strain due to cataclastic flow (e.g. Wojtal, 1989). Instead, we estimate the mesoscale elastico-frictional strain by removing the initial plastic strain (Sussman, 1995) from the overall finite strain (e.g. Ramsay and Huber, 1983). The plastic strain in the Caddy Canyon quartzites, from a few locations along the fold, have been determined by the Fry method (Fry, 1979; McNaught, 1994; Mukul, 1998).

Movement on fractures results in variable strain along the syncline, with thinning of beds in some parts and thickening in others (Table 1, Fig. 11). This is illustrated using two areas (2 and 4 in Fig. 11) with similar fracture patterns that lie in different segments across a transverse zone. The

Fig. 7. "Orientation plots" in which the fold geometry (interlimb angle) and the orientation (plunge and trend) are stereographically manipulated to match those of an adjoining area. Areas 1 and 2 are within one transverse-zone-bound-segment while Areas 2 and 4 are in two different transverse-zone-bound-segments. Conjugate-conjugate fracture sets provide the maximum shortening direction (black dots). Note the consistent shortening directions obtained from the stereographically manipulated "orientation" plots by either first removing the plunge or first unfolding. (a) Area 1 unfolded to Area 2. (b) Area 2 unfolded to Area 4. Note common up-down shortening direction.

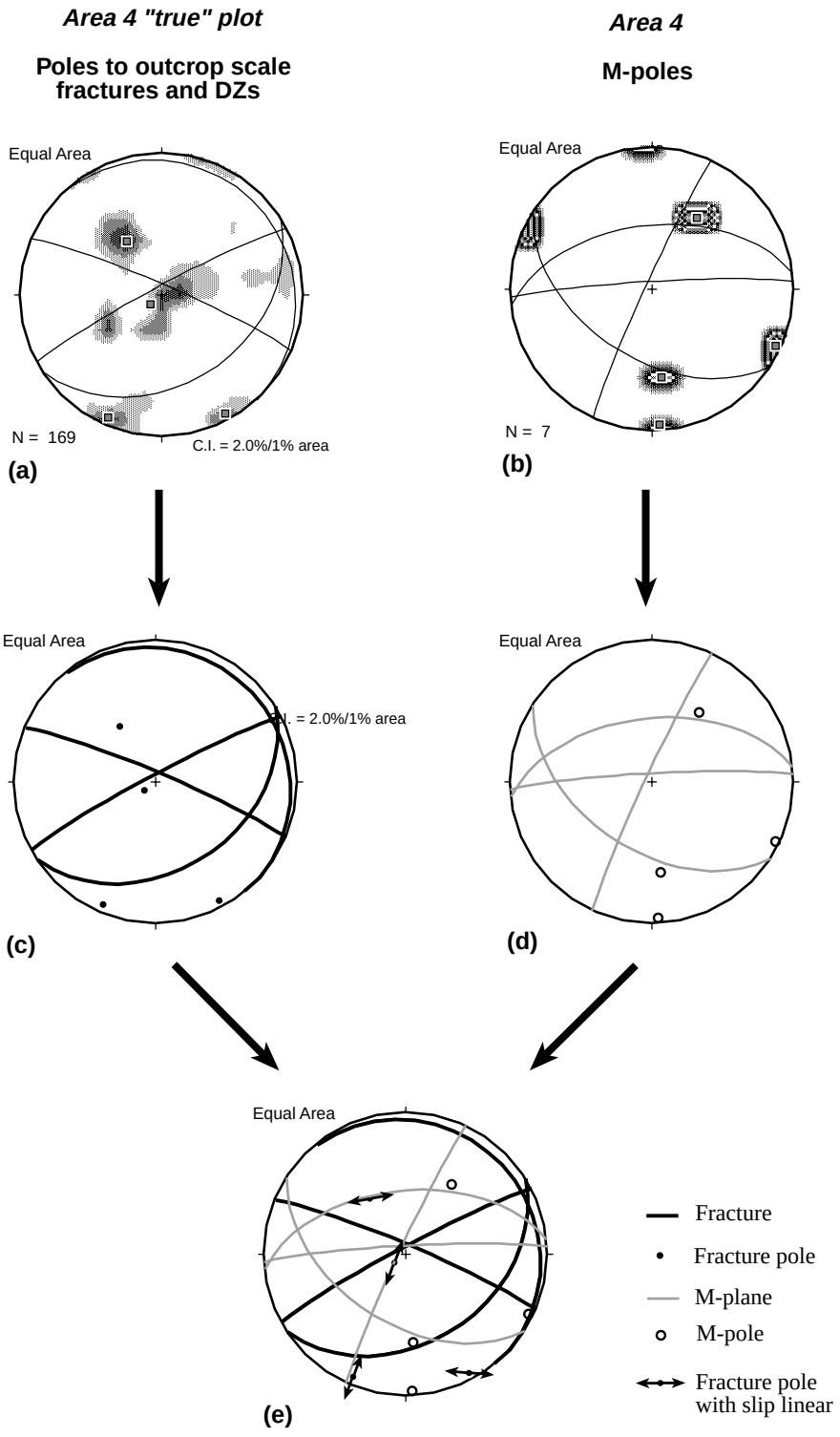

Fig. 8. (a–e) An example from area 4 illustrating the series of steps used to develop slip linear plots in order to determine motion of outcrop scale blocks. Compare slip linear plot to block motion of area 4 in Fig. 11. (a) "True plot" with great circles derived from highest fracture and DZ pole concentrations. These great circles represent active fractures and zones at that stage of folding. (b) All motion planes derived from M-pole concentrations for Area 4. (c) "True plot" fractures and DZs with their poles. (d) All M-planes and M-poles. (e) Slip-linear plot constructed from the intersection of fracture and DZ poles with M-planes. Arrows indicate possible motion along these fractures and DZs. Final motion, from the two options for each slip linear point, based on field evidence (e.g. slickenfibers and/or offset markers).

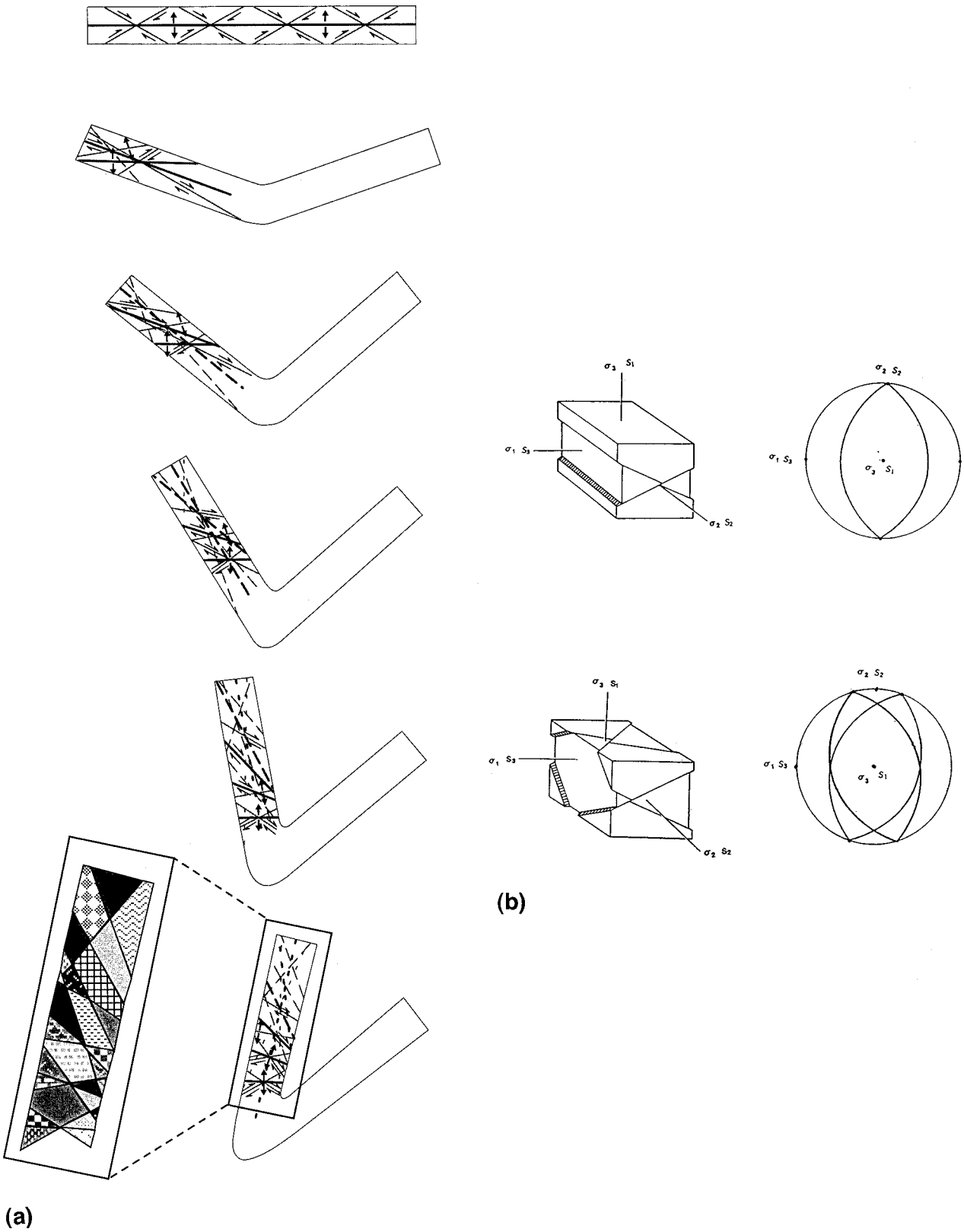

Fig. 9. (a) Plane strain model of a fold undergoing progressive tightening by limb rotation. Successive stages are shown with 20° limb rotation at each stage, assuming a constant horizontal compression direction. Thick, dark grey lines indicate fractures that originally formed as extension fractures, while thin, light grey lines are original shear fractures. Solid lines are active fractures, dashed lines are inactive fractures and dotted lines are healed fractures. "Subsystems", or various "block" sizes bounded by the cumulative active and inactive fractures are shown for the final stage of folding. (b) Conjugate fracture sets formed with plane strain in a compressive stress system (top set of figures) and conjugate-conjugate fracture sets (with orthorhombic symmetry) formed in a three-dimensional strain field with a compressive stress system (after Reches, 1975).

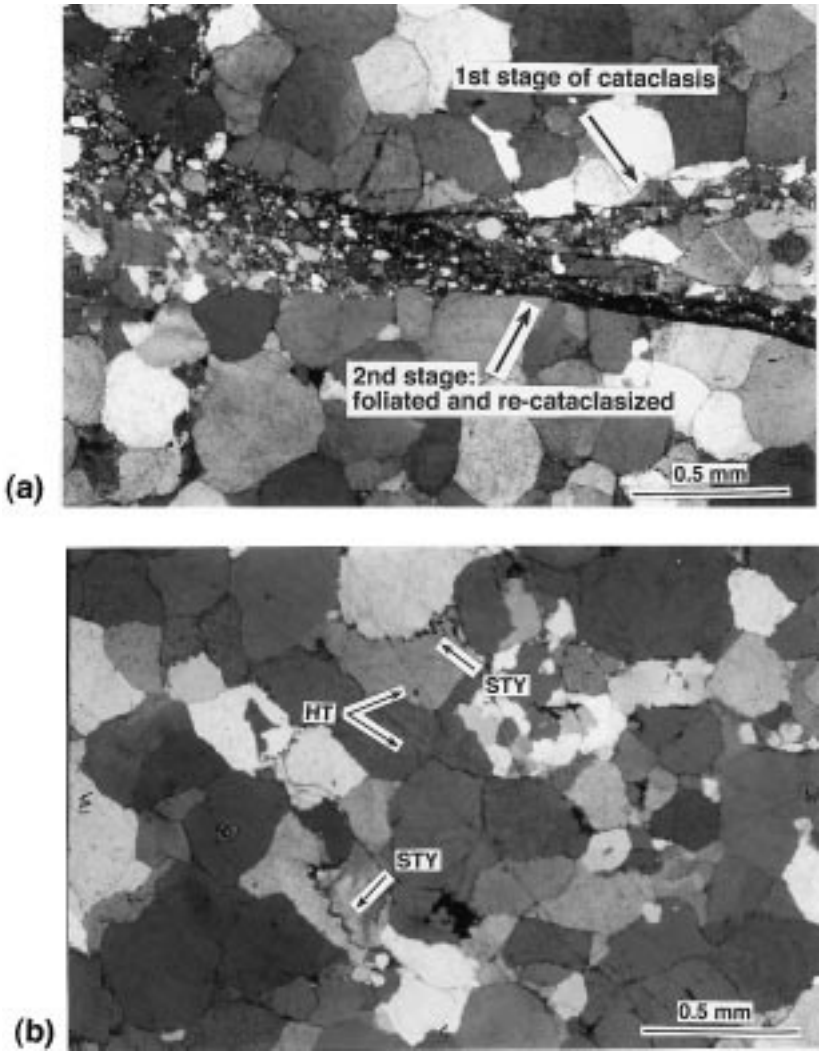

Fig. 10. (a) Photomicrograph of cataclasite zones showing recataclasized and foliated cataclasites from area 9 (see Figs. 5 and 6). (b) Photomicrograph from area 7 illustrating minimal amount of elastico-frictional deformation. Note the stylolites (STY) and healed transgranular cracks (HT).

beds in area 2 have undergone large amounts of thinning and extension (~33%, equivalent to a plane strain axial ratio of 1.77 with long axis parallel to bedding) while the beds in area 4 have undergone a large amount of thickening (~23%, equivalent to a plane strain axial ratio of 1.52 with long axis perpendicular to bedding) (Table 1). The initial plastic strain ratio in the XZ (transport) plane in area 2 is 1.08 with the long axis at 10° to bedding, and in area 4 the XZ ratio is 1.14 with the long axis at 13° to bedding. Removing the early plastic strain yields brittle deformation strain at area 2 to be 1.64 (or 28% bed-parallel stretching) and strain at area 4 to be 1.72 (or 31% bed thickening). The excess material in the fold-core at area 4 causes volume imbalance that is relieved by out-of-the-core thrusting while the CR syncline in area 2 remained continuous as fold tightening progressed by limb thinning and rotation. Clearly, similar fractures within different segments were exploited in different ways to produce distinct strain patterns.

5. Discussion

Based on our observations in the CR syncline, we have presented a model in which large-scale cataclastic flow occurs by the simultaneous development of many fractures and DZs. The volume of the resultant mesoscale blocks is much greater than the zones that bound them, so that the shape of the blocks greatly affect the behavior of the bounding zones. Although these mesoscale blocks are not 'floating' within an even larger scale DZ, the combined motion of these blocks is a form of cataclastic flow that accommodates continuous folding of the CR syncline and therefore must maintain ductility at the scale of the fold. Change in shape without significant change in volume is necessary to maintain ductility. Therefore, it follows as a geometric constraint that the DZ-bound blocks must still fit together after deformation. In other words, there must be strain compatibility (Paterson, 1978; Menendez et al., 1996). Although the DZs are discontinuities, the DZs

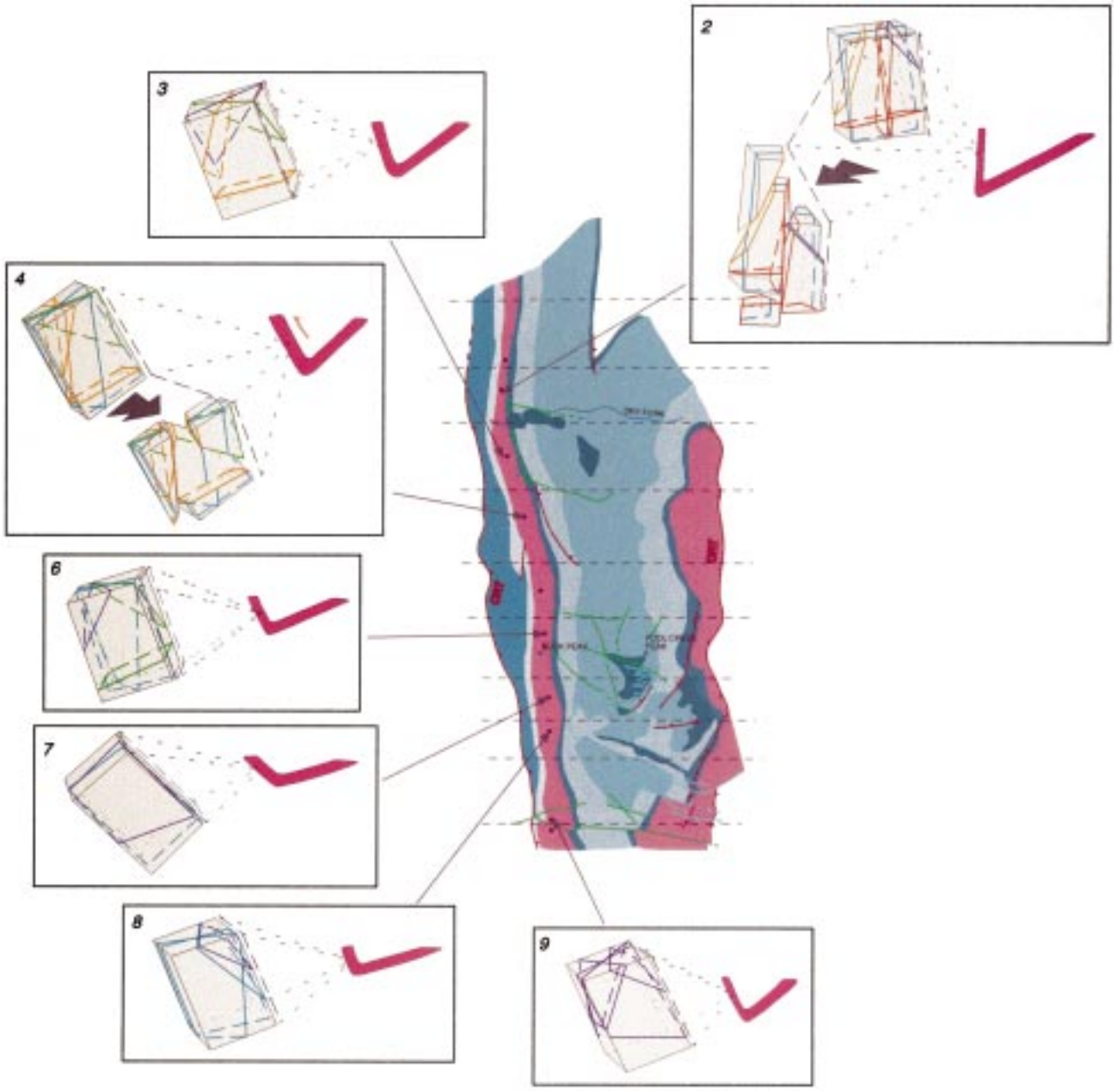

Fig. 11. Mesoscopic fracture patterns from different locations in the west limb of the Canyon Range syncline showing active fracture systems and fracture bounded blocks during the last stages of folding. Different colors indicate fractures formed at different stages of fold tightening, with cooler colors indicating earlier folding stages and warm colors indicating more advanced folding stages. Same colors in different areas indicate that the fractures formed at the same stage of folding and were reactivated as folding progressed.

bounding the blocks play an essential role in maintaining large-scale ductility and compatibility. They collectively and continuously position the blocks in the most efficient manner at each deformation stage and provide a smooth transition from block to block.

Within the plastic regime (e.g. in metals), von Mises criterion defines compatibility and requires simultaneous slip on five independent slip systems. The same compatibility constraints must be obeyed when flow takes place in any deformation regime, including cataclastic flow. Although only two pairs of conjugate slip systems (DZs) typically develop within the elastico-frictional regime when rocks are deformed, compatibility can be maintained by: (1) thinning or thickening of DZs bounding the mesoscale blocks to avoid producing gaps or overlaps, and (2) adjusting the placement and/or formation of different mesoscale block sizes to remove any gaps or overlaps. In effect, these processes produce the equivalent of five independent slip systems for continuous flow. Therefore, the necessity for five slip systems is relaxed and compatibility is still maintained.

Compatibility can also be maintained by different

deformation mechanisms being active at different scales, simultaneously. Each deformation mechanism is unique to its scale and local stresses during a phase of deformation. A cooperative, rather than a fractal, relationship exists between the deformation processes taking place at the meso and micro-scales in order to continue ductile deformation within the elastico-frictional regime. The cooperation amongst the various scales of deformation provide a means by which the overall strain progressively and smoothly changes within the deforming body. For example, the DZs maintaining large-scale cataclastic flow may also flow within the zones themselves by a different mechanism (e.g. diffusion) to maintain strain compatibility at an even smaller scale.

Cataclastic flow at any scale can only begin with the formation of a stable network of penetrative fractures and fragmentation. Before large-scale cataclastic flow occurs, a network of fractures and stable DZs must form. These form by the linking of microcracks and smaller scale DZs from various microscale DZ networks. Once the rock has fractured to form stable meso-block sizes, the blocks begin to slide past one another on a stable network of shear fractures and mesoscale DZs. As a result, the potential for continued deformation by the development or activation of other DZs outside of the stable network is substantially reduced, unless the external environment changes, such as with limb rotation. If the external environment changes, different subpopulations of large-scale DZs are activated at different stages of deformation and form stable networks to continue cataclastic flow. Evidence for the inactivity or activity of the DZs is preserved within the zones as microstructural signatures indicating hardening and softening stages, respectively. Rock deforming within the EF regime potentially provides a very complete record of the deformation history, because later structures simply cross cut, without completely obliterating, earlier structures.

6. Conclusions

1. The Canyon Range (CR) syncline trends N–S and its geometry varies from an open fold at its southern end to a tight and then overturned fold at its northern end. Based on overprinting structures and the unfolding history of the tightest part of the CR syncline, we interpret the along strike variation in geometry (tightness, thickness variation in beds and hinge shape of the fold) as equivalents of temporal stages of growth.
2. The CR syncline tightened within the elastico-frictional regime by cataclastic flow, at all scales. The deformation was accommodated by a large number of slip events on a distributed network of fractures and deformation zones (DZs) that is penetrative at the outcrop scale and can be approximated as homogeneous and continuous. Fracture- and DZ-bounding mesoscale blocks were continuously positioned in the most efficient manner at each folding stage, resulting in ductile deformation at the scale of the fold.
3. Contrasting mesofracture assembleges in different parts of the fold reflect different bulk strain histories. The fracture patterns represent many superposed increments of fracturing during fold growth.
4. Early fractures (healed or recrystallized) occur in orthorhombic sets and indicate a consistent steeply plunging shortening direction. Rotation of bedding to horizontal indicates similar sub-horizontal layer parallel shortening everywhere along the fold during early deformation.
5. Late fractures occur in orthorhombic sets and indicate similar deformation patterns within transverse-zone-bounded-segments and different patterns between transverse zones.
6. The overall strain during fold tightening is measured by the thinning or thickening of the beds at the map-scale. Approximately 30% thinning and thickening of beds is accomplished by the "jostling" motion of large blocks, bounded by mesoscale DZs. We estimate the mesoscale elastico-frictional strain in two areas by removing the initial plastic strain from the overall finite strain.

Acknowledgements

Acknowledgement is made to the donors of the Petroleum Research Fund, administered by the American Chemical Society, for support of this research under grant #33387-AC2. We thank Mary Beth Gray and Steve Wojtal for helpful discussions. We also thank the reviewers, Peter H. Hennings and Jafar Hadizadeh, and the special editor, Bill Dunne for their detailed comments, which were very useful in improving the paper.

References

Allmendinger, R.W., 1992. Fold and thrust tectonics of the western United States exclusive of the accreted terranes. In: Burchfiel, B.C., Lipman, P.W., Zoback, M.L. (Eds.), The Cordilleran Orogen, the conterminous U.S. Geological Society of America. The Geology of North America, G-3, pp. 583–608.

Allmendinger, R.W., Sharp, J.W., Von Tish, D., Serpa, L., Brown, L., Oliver, J., Kaufman, S., Smith, R.B., 1983. Cenozoic and Mesozoic structure of the eastern Basin and Range province, Utah, from COCORP seismic reflection data. Geology 11, 532–536.

Anderson, D.E., 1951. The dynamics of faulting. Oliver and Boyd, Edinburgh.

Angelier, J., 1979. Determination of the mean principal directions of stresses for a given fault population. Tectonophysics 56, T17–T26.

Armstrong, R.L., 1968. Sevier orogenic belt in Nevada and Utah. Geological Society of America Bulletin. 79, 429–458.

Arthaud, F., 1969. Methode de determination graphique des directions de raccoureissement, d'allongement et intermediaire d'une population de dailles. Compte Rendu Sommaire des seances de la Societe Geologique de France 8, 302.

Ashby, M.F., Gandhi, C., Taplin, D.M.R., 1979. Fracture mechanism maps

and their construction for F.C.C. metals and alloys. Acta Metallurgica 27, 699–729.
Bayly, M.B., 1974. An energy calculation concerning the roundness of folds. Tectonophysics 24, 291–316.
Bles, J.L., Feuga, B., 1986. The Fracture of Rocks. North Oxford Academic.
Bott, M.H.P., 1959. The mechanics of oblique slip faulting. Geol. Mag. 96, 109–116.
Boyer, S., 1992. Geometric evidence for synchronous thrusting in the southern Alberta and northwest Montana thrust belts. In: McClay, K.R (Ed.), Thrust Tectonics, pp. 337–390.
Boyer, S., Elliott, D., 1982. Thrust systems. Am. Assoc. Pet. Geol. 66, 1196–1230.
Burchfiel, B.C., Davis, G.A., 1975. Nature and controls of Cordilleran orogenesis, western United States—extensions of an earlier synthesis. American Journal of Science 275A, 363–396.
Burchfiel, B.C., Hickcox, C.W., 1972. Structural development of central Utah. In: Baer, J.L., Callaghan, E. (Eds.), Plateau-Basin and Range transition zone, central Utah. Utah Geological Association Publication 2, pp. 55–66.
Christiansen, R.F., 1952. Structure and stratigraphy of the Canyon Range: Utah. Geological Society of America Bulletin 63, 717–740.
Coogan, J.C., DeCelles, P.G., Mitra, G., Sussman, A.J., 1995. New regional balanced cross section across the Sevier desert region and the Central Utah thrust belt. Geological Society of America Rocky Mountain. Meeting Abstracts 27, 7.
DeCelles, P.G., 1994. Late Cretaceous-Paleocene synorogenic sedimentation and kinematic history of the Sevier thrust belt, northeast Utah and southwest Wyoming. Geological Society of America Bulletin 106, 32–56.
DeCelles, P.G., Lawton, T.F., Mitra, G., 1995. Timing of Sevier thrusting, central Utah. Geology 23, 699–702.
DeCelles, P.G., Mitra, G., 1995. History of the Sevier orogenic wedge in terms of critical taper models, northeast Utah and southwest Wyoming. Geological Society of America Bulletin 107, 454–462.
Etchecopar, A., Vasseur, G., Daigniers, M., 1981. An inverse problem in microtectonics for the determination of stress tensors from fault striation analysis. Journal of Structural Geology 3, 51–65.
Evans, J., 1993. Deformation mechanisms and kinematics of a crystalline cored thrust sheet. In: Schmidt, C.J., Chase, R.B., Erslev, E.A (Eds.), GSA Special Paper 280, pp. 147–162.
Fry, N., 1979. Random point distribution and strain measurement in rock. Tectonophysics 60, 89–105.
Griffith, A.A., 1920. The phenomena of rupture and flow in solids. Philosophical Transactions of the Royal Society Ser. A 221, 163–198.
Hadizadeh, B., Rutter, E.H., 1983. The low temperature brittle-ductile transition in quartzite and the occurrence of cataclastic flow in nature. Geologische Rundschau 72, 493–509.
Hancock, P.L., 1985. Brittle microtectonics: principles and practice. Journal of Structural Geology 7, 437–457.
Higgins, J.M., 1982. Geology of the Champlin Peak quadrangle, Juab and Millard counties, Utah. Brigham Young University Geology Studies 29, 40–58.
Hintze, L.F., 1988. Geologic history of Utah. Brigham Young University Geology Studies Special Publication 7, 202.
Holladay, J.C., 1983. Geology of the northern Canyon Range, Millard and Juab counties, Utah. Brigham Young University Geology Studies 31, 1–28.
Jamison, W.R., Stearns, D.W., 1982. Tectonic deformation of the Windgate sandstone, Colorado National Monument. Bull. Am. Ass. Petrol. Geol. 66, 2584–2608.
Lawton, T.F., 1982. Lithofacies correlations within the Upper Cretaceous Indianola Group. In: Nielson, D.L. (Ed.), Overthrust Belt of Utah. Utah Geol. Assoc. Publication, 10, pp. 199–213.
Lawton, T., 1985. Style and timing of the frontal structures, Sevier thrust belt, central Utah. American Association of Petroleum Geology Bulletin 69, 1145–1159.
Lawton, T.F., Sprinkel, D.F., DeCelles, P.G., Mitra, G., Sussman, A.J., Weiss, M.P., 1997. Sevier thrust belt central-Utah: Sevier Desert to Wasatch Paleau. In: Link, K.P., Kowallis, B.J. (Eds.), BYU Geology Studies Field Trip Guide Book pt. II, Geological Society of America Annual Meeting, pp. 33–68.
McNaught, M.A., 1994. Modifying the normalized Fry method for aggregates of non-eliptical grains. Journal of Structural Geology 16, 493–503.
Menendez, B., Zhu, W., Wong, T., 1996. Micromechanics of brittle faulting and cataclastic flow in Berea sandstone. Journal of Structural Geology 18, 1–16.
Millard Jr., A.W., 1983. Geology of the southwestern quarter of the Scipio North (15-minute) quadrangle, Millard and Juab counties, Utah. Brigham Young University Geology Studies 30, 59–81.
Miller, D.M., Nilsen, T.H., Bilodeau, W.L., 1992. Late Cretaceous to early Eocene geologic evolution of the U. S. Cordillera. In: Burchfiel, B.C., Lipman, P.W., Zoback, M.L. (Eds.), The Cordilleran Orogen, the conterminous U.S. Geological Society of America, The Geology of North America, G-3, pp. 205–260.
Mitra, G., 1978. Ductile deformation zones and mylonites: The mechanical processes involved in the deformation of crystalline basement rocks. American Journal of Science 278, 1057–1084.
Mitra, G., 1984. Brittle to ductile transition due to large strains along the White Rock thrust, Wind River Mountains, Wyoming. Journal of Structural Geology 6, 51–61.
Mitra, G., 1992. Deformation of granitic basement rocks along fault zones at shallow to intermediate crustal levels. In: Mitra, S., Fisher, G.W. (Eds.), Structural Geology of Fold and Thrust Belts, pp. 123–144.
Mitra, G., 1997. Evolution of salients in a fold-and-thrust belt: the effects of sedimentary basin geometry, strain distribution and critical taper. In: Sengupta, S. (Ed.), Evolution of Geological Structures in Micro- to Macro-scales. Chapman & Hall, London, pp. 59–90.
Mitra, G., Pequera, N., Sussman, A.J., DeCelles, P.G., 1994. Evolution of structures in the Canyon Range thrust sheet (Sevier fold-and-thrust belt) based on field relations and microstructural studies. Geological Society of America Annual Meeting. Abstracts 26, A527.
Mitra, G., Sussman, A.J., Pequera, N., DeCelles, P.G., Coogan, J.C., 1995. Structural evolution of the Canyon Range, Central Utah Sevier orogenic wedge: implications for critical taper during thrusting. Geological Society of America Rocky Mountain Meeting Abstracts 27, 47.
Mitra, G., Sussman, A.J., 1997. Structural evolution of connecting splay duplexes and their implications for critical taper: an example based on geometry and kinematics of the Canyon Range culmination, Sevier Belt, central Utah. Journal of Structural Geology 19, 503–521.
Mukul, M., 1998. A spatial statistics approach to the quantification of finite strain variation in penetratively deformed thrust sheets: an example from the Sheeprock Thrust Sheet Sevier Fold-and-Thrust belt, Utah. Journal of Structural Geology 20, 371–384.
Paterson, M.S., 1978. Experimental Rock Deformation—the Brittle Field. Springer-Verlag, New York.
Pequera, N. 1991. Growth history of a fault-propagation fold: An example from the Canyon Range, central Utah. M.S. Essay, University of Rochester, 23 p.
Pequera, N., Mitra, G., Sussman, A.J., 1994. The Canyon Range thrust sheet in the Sevier fold-and-thrust belt of central Utah: deformation history based on structural analysis. Geological Society of America Rocky Mountain Meeting Abstracts 26, 58.
Price, N.J., 1966. Fault and Joint Development in Brittle and Semi-Brittle Rocks. Pergamon Press, Oxford.
Price, R.A., 1967. The tectonic significance of mesoscopic subfabrics in the southern Rocky Mountains of Alberta and British Colombia. Canadian Journal of Earth Sciences 4, 39–70.
Prucha, J.J., Graham, J.A., Nickelsen, R.P., 1965. Basement controlled deformation in Wyoming Province of Rocky Mountains foreland. Bulletin of the American Association of Petroleum Geologists 49, 966–992.
Ramsay, J.G., 1967. Folding and fracturing of rocks. McGraw-Hill Book Co., New York.

Ramsay, J.G., Huber, M.I., 1983. The Techniques of Modern Structural Geology Volume 1: Strain Analysis. Academic Press, New York.

Reches, Z., 1978. Analysis of faulting in three dimensional strain field. Tectonophysics 47, 109–129.

Reches, Z., 1983. Faulting of rocks in three-dimensional strain fields: II. Theoretical analysis. Tectonophysics 95, 133–156.

Reches, Z., Dieterich, J.H., 1983. Faulting of rocks in three dimensioanl strain fields: 1. Failure of rocks in polyaxial, servo-control experiments. Tectonophysics 95, 111–132.

Royse, F., 1993. Case of the phantom foredeep: Early Cretaceous in west-central Utah. Geology, v. 21, 133–136.

Rutter, E.H., 1986. On the nomenclature of mode of failure transitions in rocks. Tectonophysics 122, 381–387.

Schmid, S.M., 1982. Microfabric studies as indicators of deformation mechanisms and flow laws operative in mountain building. In: Hsu, K.J. (Ed.), Mountain Building Processes. Academic Press, pp. 95–110.

Schmid, S.M., Handy, M.R., 1991. Towards a genetic classification of fault rocks: Geological usage and tectonophysical implications. In: Muller, D.W., McKenzie, J.A., Weissert, H. (Eds.), Controversies in Modern Geology: Evolution of Geological Theories in Sedimentology, Earth History and Tectonics. Academic Press, London.

Schwartz, R.K., DeCelles, P.G., 1988. Cordilleran foreland-basin evolution and synorogenic sedimentation in response to interactive Cretaceous thrusting and reactivated foreland partitioning. In: Schmidt, C.J., Perry, W.J. (Eds.), Interaction of the Rocky Mountain Foreland & Cordilleran Thrust Belt. Geol. Soc. of America Memoir, 171, pp. 489–514.

Schonborn, G., 1992. Alpine tectonics and kinematic models of the central southern Alps, Memorie di Scienze Geologiche Institut du Geologia e Mineralogia de ll. Universita de Padova 44, 229–393.

Sibson, R.H., 1977. Fault rocks and fault mechanics. Journal of the Geological Society of London 133, 191–213.

Smith, R.B., Bruhn, R.L., 1984. Intrapalte extensional tectonics of the eastern Basin-Range; inferences on structural style from seismic reflection data, regional tectonics, and thermal mechanical models of brittle-ductile deformation. Journal of Geophysical Research 89, 5733–5762.

Standlee, L.A., 1982. Structure and stratigraphy of Jurassic rocks in central Utah: Their influence on tectonic development of the Cordilleran foreland thrust belt. In: Powers, R.B. (Ed.), Geologic studies of the Cordilleran foreland thrust belt. Rocky Mountain Association of Geologists, pp. 357–382.

Stearns, D.W., 1975. Laramide basement deformation in the Bighorn basin—the controlling factor for structures in layered rocks, Wyoming Geological Assoc. Guidebook, 27th annual field conference, pp. 149–158.

Stearns, D.W., 1978. Faulting and forced folding in the Rocky Mountains foreland, In: Laramide folding Associated with Basement Block Faulting in western United States. GSA Memoir 151, 1–38.

Sussman, A.J., 1995. Geometry, deformation history and kinematics in the footwall of the Canyon Range thrust, central Utah. M.S. thesis, Universtiy of Rochester, 120 p.

Sussman, A.J., Mitra, G., 1995a. Deformation patterns in the footwall of the Canyon Range thrust, central Utah: implications for Sevier fold-and-thrust belt development. Geological Society of America Rocky Mountain Meeting Abstracts 27, 57.

Sussman, A.J., Mitra, G., 1995b. Structural evolution of a connecting splay duplex: an example based on field and microstructural studies in the footwall of the Canyon Range thrust, Utah. Geological Society of America Rocky Mountain Meeting Abstracts 27, 122.

Tullis, J., Schmid, S., Etheridge, M., 1982. Short course on ductile deformation mechanisms and microstructures, Geological Society of America Annual Meeting.

Twiss, R.J., Moores, E.M., 1992. Structural Geology. W.H. Freeman and Company.

Twiss, R.J., Unruh, J.R., 1998. Analysis of fault slip inversions: Do they constrain stress or strain rate? Journal of Geophysical Research 103, 12205–12222.

Underwood, E.E., 1970. Quantitative Stereology. Addison-Wesley Publishing Company.

Villien, A., Kligfield, R.M., 1986. Thrusting and synorogenic sedimentation in central Utah. In: Peterson, J.A. (Ed.), Paleotectonics and sedimentation in the Rocky Mountain region, United States. American Association of Petroleum Geology Memoir, pp. 281–308.

Wise, D., 1964. Microjointing in basement, middle Rocky Mountains of Montana and Wyoming. GSA Bulletin 75, 287–305.

Wojtal, S., 1989. Measuring displacement gradients and strains in rocks. Journal of Structural Geology, 11, 669–678.

Wojtal, S., Mitra, G., 1986. Strain hardening and strain softening in fault zones from foreland thrusts. Geological Society of America Bulletin 97, 674–687.

Wojtal, S. & Mitra, G., 1988. Nature of deformation in some fault rocks from Appalachian thrusting, In: Mira, G. and Wojtal, S. (Eds.), Geometries and Mechanisms of Thrusting with Special Reference to the Appalachians. GSA Special Paper 222.

Yonkee, W.A., Mitra, G., 1993. Comparision of basement deformation styles in the Rocky Mountain Foreland and Sevier Orogenic Belt. In: Schmidt, C., Chase, R. & Erslev, E. (Eds.), Basement behavior in Rocky Mountain foreland structure. Geological Society of America Special Paper 280, 197–228.